Joint Radar and Communication Design: Applications, State-of-the-art, and the Road Ahead

Fan Liu, *Member, IEEE,* Christos Masouros, *Senior Member, IEEE,* Athina P. Petropulu, *Fellow, IEEE,* Hugh Griffiths, *Fellow, IEEE* and Lajos Hanzo, *Fellow, IEEE*

(Invited Paper)

***Abstract*—Sharing of the frequency bands between radar and communication systems has attracted substantial attention, as it can avoid under-utilization of otherwise permanently allocated spectral resources, thus improving efficiency. Further, there is increasing demand for radar and communication systems that share the hardware platform as well as the frequency band, as this not only decongests the spectrum, but also benefits both sensing and signaling operations via the full cooperation between both functionalities. Nevertheless, its success critically hinges on high-quality joint radar and communication designs. In the first part of this paper, we overview the research progress in the areas of radar-communication coexistence and dual-functional radar-communication (DFRC) systems, with particular emphasis on the application scenarios and the technical approaches. In the second part, we propose a novel transceiver architecture and frame structure for a DFRC base station (BS) operating in the millimeter wave (mmWave) band, using the hybrid analog-digital (HAD) beamforming technique. We assume that the BS is serving a multi-antenna user equipment (UE) over a mmWave channel, and at the same time it actively detects targets. The targets also play the role of scatterers for the communication signal. In that framework, we propose a novel scheme for joint target search and communication channel estimation relying on omni-directional pilot signals generated by the HAD structure. Given a fully-digital communication precoder and a desired radar transmit beampattern, we propose to design the analog and digital precoders under non-convex constant-modulus (CM) and power constraints, such that the BS can formulate narrow beams towards all the targets, while pre-equalizing the impact of the communication channel. Furthermore, we design a HAD receiver that can simultaneously process signals from the UE and echo waves from the targets. By tracking the angular variation of the targets, we show that it is possible to recover the target echoes and mitigate its potential interference imposed on the UE signals, even when the radar and communication signals share the equivalent signal-to-noise ratio (SNR). The feasibility and the efficiency of the proposed approaches in realizing DFRC are verified via numerical simulations. Finally, our discussions are summarized by overviewing the open problems in the research field of communication and radar spectrum sharing (CRSS).**

***Index Terms*—Radar-communication spectrum sharing, dual-functional radar-communication, hybrid beamforming, mmWave.**

Manuscript received June 1, 2019; revised October 5, 2019, December 5, 2019 and January 21, 2020; accepted February 8, 2020. This work was supported in part by the Marie Skłodowska-Curie Individual Fellowship under Grant No. 793345, in part by the Engineering and Physical Sciences Research Council (EPSRC) of the UK Grant number EP/S026622/1, and in part by the UK MOD University Defence Research Collaboration (UDRC) in Signal Processing. L. Hanzo would like to acknowledge the financial support of the EPSRC projects EP/Noo4558/1, EP/PO34284/1, COALESCE, of the Royal Society's Global Challenges Research Fund Grant as well as of the European Research Council's Advanced Fellow Grant QuantCom. A. P. Petropulu would like to acknowledge the financial support of the US National Science Foundation under grant CCF-1526908. The associate editor coordinating the review of this paper and approving it for publication was D. I. Kim. (*Corresponding author: Fan Liu.*)

F. Liu, C. Masouros and H. Griffiths are with the Department of Electronic and Electrical Engineering, University College London, London, WC1E 7JE, UK (e-mail: fan.liu@ucl.ac.uk, chris.masouros@ieee.org, h.griffiths@ieee.org).

A. P. Petropulu is with the Department of Electrical and Computer Engineering, Rutgers, the State University of New Jersey, 94 Brett Road, Piscataway, NJ 08854, United States (e-mail: athinap@rutgers.edu).

L. Hanzo is with the School of Electronics and Computer Science, University of Southampton, Southampton SO17 1BJ, UK. (e-mail: lh@ecs.soton.ac.uk).

I. Introduction

A. Background

GIVEN the plethora of connected devices and services, the frequency spectrum is becoming increasingly congested with the rapid growth of the wireless communication industry. As a consequence, the auction price of the available wireless spectrum has experienced a sharp rise during recent years. For example, since 2015, mobile network operators in the UK have been required to pay a combined annual total of £80.3 million for the 900 MHz and £119.3 million for the 1800 MHz band, employed for voice and data services using a mix of 2/3/4G technologies [1]. Meanwhile in Germany, the regulator Bundesnetzagentur revealed that the total in the auction of 4 frequency bands for mobile network operators exceeded €5 billion [2]. The US Federal Communications Commission (FCC) completed its first 5G auction, with a sale of 28 GHz spectrum licences raising $702 million [3]. By 2025, the number of connected devices worldwide is predicted to be 75 billion [4], which further emphasizes impending need for extra spectral resources. In view of this, network providers are seeking opportunities to reuse spectrum currently restricted to other applications. The *radar bands* are among at the best candidates to be shared with various communication systems due to the large portions of spectrum available at radar frequencies [5].

Radar has been developed for decades since its birth in the first half of the 20th century. Modern radar systems are deployed worldwide, with a variety of applications including air traffic control (ATC), geophysical monitoring, weather observation as well as surveillance for defense and security. Below 10 GHz, a large portion of spectral resources has been primarily allocated to radar, but at the current state-of-the-art new cohabitation options with wireless communication systems, e.g. 5G NR, LTE and Wi-Fi [5]. At the higher

TABLE I
LIST OF ACRONYMS

AoA	Angle of Arrival
AoD	Angle of Departure
ATC	Air Traffic Control
AV	Autonomous Vehicle
BS	Base Station
CM	Constant Modulus
CRSS	Communication and Radar Spectrum Sharing
CRB	Cramér-Rao Bound
CSI	Channel State Information
DL	Downlink
DP	Downlink Pilot
DFRC	Dual-functional Radar-Communication
GNSS	Global Navigation Satellite-based Systems
GP	Guard Period
HAD	Hybrid Analog-Digital Beamforming
ICSI	Interference Channel State Information
LTE	Long-Term Evolution
LPI	Low-probability of Intercept
LoS	Line-of-Sight
MIMO	Multi-Input-Multi-Output
mmWave	Millimeter Wave
mMIMO	Massive MIMO
MUI	Multi-user Interference
MU-MIMO	Multi-user MIMO
NR	New Radio
NSP	Null-space Projection
NLoS	Non Line-of-Sight
PRF	Pulse Repetition Frequency
PRI	Pulse Repetition Interval
RCC	Radar-Communication Coexistence
RCS	Radar Cross Section
RF	Radio Frequency
RFID	Radio Frequency Identification
SIC	Successive Interference Cancellation
SINR	Signal-to-Interference-plus-Noise Ratio
SNR	Signal-to-Noise Ratio
SVD	Singular Value Decomposition
TDD	Time-division Duplex
UAV	Unmanned Areial Vehicle
UE	User Equippment
UL	Uplink
UP	Uplink Pilot
V2X	Vehicle-to-Everything
WPS	WiFi Positioning System

TABLE II
LIST OF NOTATIONS

N_{BS}	Number of antennas at the BS
N_{UE}	Number of antennas at the UE
N_{RF}	Number of RF chains at the BS
K	Number of all the targets
L	Number of the communication scatterers
T_P	Length of the pilots
T_{DL}	Length of the DL data block
T_{UL}	Length of the UL data block
P_T	Transmit power budget
α_k	Reflection coefficient of the *k*th target
θ_k	AoA of the *k*th target relative to the BS
p_k	Range bin index of the *k*th target in the radar channel
q_k	Doppler bin index of the *k*th target in the radar channel
β_l	Scattering coefficient of the *l*th scatterer
θ_l	DL AoA (UL AoD) of the *l*th communication path
ϕ_l	DL AoD (UL AoA) of the *l*th communication path
Θ	The set of all the $\theta_k, k = 1, ..., K$
Θ_1	The set of all the $\theta_l, l = 1, ..., L$, $\Theta_1 \subseteq \Theta$
Θ_2	The complementary set of Θ_1, $\Theta_2 = \Theta \backslash \Theta_1$
Φ	The set of all the $\phi_l, l = 1, ..., L$
$\tilde{p}_l$	Range bin index of the *l*th communication path
$\tilde{q}_l$	Doppler bin index of the *l*th communication path
P	Number of range bins
Q	Number of half of the Doppler bins
Ω	Maximum Doppler angular frequency
$\boldsymbol{\alpha}$	The vector that contains $\alpha_k, k = 1, ..., K$
$\boldsymbol{\beta}$	The vector that contains $\beta_l, l = 1, ..., L$
$\mathbf{a}(\theta)$	Steering vector at the BS
$\mathbf{b}(\phi)$	Steering vector at the UE
$\mathbf{A}(\Theta)$	Steering matrix at the BS
$\mathbf{B}(\Phi)$	Steering matrix at the UE
$\mathbf{J}_p$	Temporal shifting matrix associated with the *p*th range bin
$\mathbf{d}_q$	Doppler shift vector associated with the *q*th Doppler bin
$\mathbf{S}_{DP}$	DL pilot matrix
$\mathbf{S}_{UP}$	UL pilot matrix
$\mathbf{S}_{BB}$	DL Baseband signal matrix
$\mathbf{F}_{RF}$	Analog precoding matrix at the BS
$\mathbf{F}_{BB}$	Digital precoding matrix at the BS
$\mathbf{F}_D$	The overall hybrid precoding matrix, $\mathbf{F}_D = \mathbf{F}_{RF}\mathbf{F}_{BB}$
$\mathbf{F}_{UE}$	Fully-digital ZF precoding matrix at the UE
$\mathbf{F}_{BS}$	Fully-digital ZF precoding matrix at the BS
$\mathbf{W}_{RF}$	Analog combination matrix at the BS
$\mathbf{W}_{BB}$	Baseband combination matrix at the BS
$\mathbf{W}_{UE}$	Fully-digital ZF combination matrix at the UE

frequencies such as the mmWave band, the communication and radar platforms are also expected to achieve harmonious coexistence or even beneficial cooperation in the forthcoming 5G network and beyond. Nevertheless, with the allocation of the available frequency bands to the above wireless technologies, the interference in the radar bands is on the rise, and has raised concerns both from governmental and military organizations for the safeguarding of critical radar operations [6]–[10]. To this end, research efforts are well underway to address the issue of communication and radar spectrum sharing (CRSS).

In general, there are two main research directions in CRSS: 1) Radar-communication coexistence (RCC) and 2) Dual-functional Radar-Communication (DFRC) system design [11]. The first category of research aims at developing efficient interference management techniques, so that the two systems can operate without unduly interfering with each other. On the other hand, DFRC techniques focus on designing joint systems that can simultaneously perform wireless communication and remote sensing. In contrast to the RCC technique which relies on sharing the information between radar and

communication systems, or on an extra control center with the coordination capability, DFRC design benefits both sensing and signaling operations via real-time cooperation, decongests the RF environment, and allows a single hardware platform for both functionalities. This type of work has been extended to numerous novel applications, including vehicular networks, indoor positioning and covert communications [12]–[14].

Below we present existing, or potential application scenarios of CRSS from both civilian and military perspectives.

B. Civilian Applications

1) Coexistence of radar and wireless systems

As discussed above, CRSS has originally been motivated by the need for the coexistence of radar and commercial wireless systems. Next, we provide examples of coexisting systems in various bands.

- *L-band (1-2 GHz)*: This band is primarily used for long-range air-surveillance radars, such as Air Traffic Control (ATC) radar, which transmits high-power pulses with modest bandwidth. The same band, however, is also used by 5G NR and FDD-LTE cellular systems as well as the Global Navigation Satellite System (GNSS) both in their downlink (DL) and uplink (UL) [15].
- *S-band (2-4 GHz)*: This band is typically used for airborne early warning radars at considerably higher transmit power [16]. Some long-range weather radars also operate in this band due to moderate weather effects in heavy precipitation [5]. Communication systems present in this band include 802.11b/g/n/ax/y WLAN networks, 3.5 GHz TDD-LTE and 5G NR [17].
- *C-band (4-8 GHz)*: This band is more sensitive to weather patterns. Therefore, it is assigned to most types of weather radars for locating light/medium rain [5]. On the same band, radars are operated for battlefield/ground surveillance and vessel traffic service (VTS) [5]. Wireless systems in this band mainly include WLAN networks, such as 802.11a/h/j/n/p/ac/ax [18].
- *MmWave band (30-300 GHz)*[1]: This band is conventionally used by automotive radars for collision detection and avoidance, as well as by high-resolution imaging radars [19]. However, it is bound to become busier, as there is a huge interest raised by the wireless community concerning mmWave communications, which are soon to be finalized as part of the 5G NR standard [20]. Currently, the mmWave band is also exploited by the 802.11ad/ay WLAN protocols [18].

Among the above coexistence cases, the most urgent issues arise due to interference between base stations and ATC radars [15]. In the forthcoming 5G network, the same problem still remains to be resolved. For reasons of clarity, we summarize the above coexistence cases in TABLE III.

2) 5G mmWave localization for vehicular networks

In next-generation autonomous vehicle (AV) networks, vehicle-to-everything (V2X) communication will require low-latency Gbps data rates; while general communications can deal with hundreds of ms delays, AV-controlled critical applications require delays of the order of tens of ms [12]. In the same scenario, radar sensing should be able to provide robust, high-resolution obstacle detection on the order of several centimeters. At the time of writing, vehicular localization and networking schemes are mostly built upon GNSS or default standards such as dedicated short-range communication (DSRC) [21] and the D2D mode of LTE-A [19]. While these approaches do provide basic V2X functionalities, they are unable to fulfill the demanding requirements mentioned above. As an example, the 4G cellular system provides localization information at an accuracy of the order of 10m, at a latency often in excess of 1s, and is thus far from ensuring driving safety [12].

It is envisioned that the forthcoming 5G technology, exploiting both massive MIMO antenna arrays and the mmWave spectrum, will be able to address the future AV network requirements [22], [23]. The large bandwidth available in the mmWave band would not only enable higher data rates, but would also significantly improve range resolution. Furthermore, large-scale antenna arrays are capable of formulating "pencil-like" beams that accurately point to the directions of interest; this could compensate for the path-loss encountered by mmWave signals, while potentially enhancing the angle of arrival (AoA) estimation accuracy. More importantly, as the mmWave channel is characterized by having only a few multipath components, there is far less clutter interference imposed on target echoes than that of the rich scattering channel encountered in the sub-6GHz band, which is thus beneficial for localization of vehicles [12].

For all of the advantages mentioned in Sec. I-A, it would make sense to equip vehicle or road infrastructure sensors with joint radar and communication functionalities. While the current DFRC system has considered sensors with dual functionality, those were mainly for the lower frequency bands, and cannot be easily extended to the V2X scenario. However, several problems need to be investigated in that context, such as specific mmWave channel models and constraints.

3) Wi-Fi based indoor localization and activity recognition

Indoor positioning technologies represent a rapidly growing market, and thus are attracting significant research interest [13], [24]. While GNSS is eminently suitable for outdoor localizations, its performance degrades drastically in an indoor environment. Conventional through-wall radar (TWR) systems have shown good performance for indoor target detection [25], [26]. Wi-Fi based positioning systems (WPS) have also emerged as promising solutions, due to their low cost and ubiquitous deployment, while requiring no additional hardware [13]. In WPS, the Wi-Fi access point (AP) receives the signal sent from the UE, and then locates the UE based on the estimate of the time of arrival (ToA) and AoA parameters. Alternatively, localization information can also be obtained by measuring the received signal strength (RSS) and by exploiting its fingerprint properties (frequency response, I/Q signal strength, etc.), which are then associated with a possible location in a pre-measured fingerprint database [27]–[29].

To gain more detailed information concerning a target such as human behavior, the receiver can process the sig-

[1]Typically, communication systems operated close to 30GHz (e.g. 28GHz) are also referred to as mmWave systems.

TABLE III
RADAR-COMMUNICATION COEXISTENCE CASES

Frequency Band	Radar Systems	Communication Systems
L-band (1-2GHz)	Long-range surveillance radar, ATC radar	LTE, 5G NR
S-band (2-4GHz)	Moderate-range surveillance radar, ATC radar, airborne early warning radar	IEEE 802.11b/g/n/ax/y WLAN, LTE, 5G NR
C-band (4-8GHz)	Weather radar, ground surveillance radar, vessel traffic service radar	IEEE 802.11a/h/j/n/p/ac/ax WLAN
MmWave band (30-300GHz)	Automotive radar, high-resolution imaging radar	IEEE 802.11ad/ay WLAN, 5G NR

nal reflected/scattered by the human body based on specific transmitted signals. Such system is more similar to a *bistatic radar* than to conventional WPS. The micro-Doppler shift caused by human activities can be further extracted from the channel state information (CSI) of the Wi-Fi, and analyzed for recognizing human actions [30], [31]. Potential applications of such techniques go far beyond the conventional indoor localization scenarios, which include health-care for elderly people, contextual awareness, anti-terrorism actions and Internet-of-Things (IoT) for smart homes [30], [32], [33]. It is worth highlighting that a similar idea has been recently applied by the *Soli* project as part of the Google Advanced Technology and Projects (ATAP), where a mmWave radar chip has been designed for finger-gesture recognition by exploiting the micro-Doppler signatures, hence enabling touchless human-machine interaction [34].

The above technology can be viewed as a particular radar/sensing functionality incorporated into a Wi-Fi communication system, which again falls into the area of DFRC. Consequently, sophisticated joint signal processing approaches need to be developed for realizing simultaneous localization and communications.

4) Unmanned aerial vehicle (UAV) communication and sensing

UAVs have been proposed as aerial base stations to a range of data-demanding scenarios such as concerts, football games, disasters and emergency scenarios [35]. It is worth noting that in all of these applications, communication and sensing are a pair of essential functionalities. In contrast to the commonly-used camera sensor on the typical UAV platforms which are sensitive to environmental conditions, such as light intensity and weather, radio sensing is more robust and could thus be incorporated into all-weather services. Additionally, radio sensing could be adopted in drone clusters for formation flight and collision avoidance [36]. While both communication and sensing techniques have been individually investigated over the past few years, the dual-functional design aspect remains widely unexplored for UAVs. By the shared exploitation of the hardware between sensors and transceivers, the payload on the UAV is minimized, which increases its mobility/flexibility, while reducing the power consumption [37].

5) Others

Apart from the aforementioned research contributions, there are also a number of interesting scenarios, where CRSS based techniques could find employment, which include but are not limited to:

- *Radio Frequency Identification (RFID):* A typical RFID system consists of a reader, reader antenna array and tags. Tags can either be passive or active depending on whether they carry batteries. To perform the identification, the reader firstly transmits an interrogation signal to the tag, which is modulated by the tag and then reflected back to the reader, giving a unique signature generated by the particular variation of the tag's antenna load [38]. The RFID based sensing is carried out by establishing a cooperative communication link between the reader and the tag. Hence this combines radar and communication techniques to a certain degree.
- *Medical sensors:* To monitor the health conditions of patients, bio-sensors may be embedded in the human body. As these sensors support only low-power sensing relying on their very limited computational capability, the measured raw data has to be transmitted to an external device for further processing. Joint sensing and communication is still an open problem in that scenario [39].
- *Radar as a relay:* In contrast to classic wireless communications, most radar waveforms are high-powered and strongly directional. These properties make the radar a suitable communication relay, which can amplify and forward weak communication signals to remote users [40]. Again, joint radar and communication relaying can play a significant role here.

C. Military Applications

1) Multi-function RF systems

The development of shipborne and airborne RF systems, including communication, electronic warfare (EW) and radar, has been historically separated from each other. The independent growth of these sub-systems led to significant increase in the volume and weight of the combat platform, as well as in the size of the antenna array. This results in a larger radar cross-section (RCS) and a consequently increased detectability by adversaries. Moreover, the coexistence of such sub-systems inevitably causes electromagnetic compatibility issues, which may impose serious mutual interference on the existing subsystems. To address these problems, the Advanced Multi-function Radio Frequency Concept (AMRFC) project was launched by the Defense Advanced Research Projects Agency (DARPA) in 1996, whose aim was to design integrated RF systems capable of simultaneously supporting multiple functions mentioned above [41], [42]. In 2009, the Office of

TABLE IV
APPLICATIONS OF THE CRSS TECHNOLOGY

Civilian Applications	Radar-comms coexistence, V2X network, WiFi localization, UAV comms and sensing, RFID, Medical sensors, Radar relay, etc.
Military Applications	Multi-function RF system, LPI comms, UAV comms and sensing, Passive radar, etc.

Naval Research (ONR) sponsored a follow-up project namely the Integrated Topside (InTop) program [43], with one of its goals to further develop wideband RF components and antenna arrays for multi-function RF systems based on the outcome of AMRFC.

Clearly, the fusion of radar and communication subsystems is at the core of the above research. By realizing this, a dedicated project named as "Shared Spectrum Access for Radar and Communications (SSPARC)" was funded by DARPA in 2013, and was further developed into the second phase in 2015 [8]. The purpose of this project was to release part of the sub-6GHz spectrum which is currently allocated to radar systems for shared use by radar and wireless communications. By doing so, SSPARC aims for sharing the radar spectrum not only with military communications, but also with civilian wireless systems, which is closely related to the coexistence cases discussed in Sec. I-B.

2) Military UAV applications

In addition to the civilian aspect mentioned above, UAVs have also been considered as an attractive solution to a variety of military missions that require high mobility, flexibility and covertness. Such tasks include search and rescue, surveillance and reconnaissance as well as electronic countermeasures [44]–[46], all of which need both sensing and communication operations. Similar to its civilian counterpart, the integration of the two functionalities could significantly reduce the payload as well as the RCS of the UAV platform.

On the other hand, UAVs can also be a threat to both infrastructures and people, as it might be used to carry out both physical and cyber attacks. Moreover, even civilian UAVs can impose unintentional but serious danger if they fly into restricted areas [47]. To detect and track unauthorized UAVs, various techniques such as radar, camera and acoustic sensors have been employed. Nevertheless, a dedicated equipment specifically conceived for sensing UAVs could be expensive to deploy [48]. Therefore, there is a growing demand to utilize existing communication systems, such as cellular BSs, to monitor unauthorized UAVs while offering wireless services to authorized UEs, which needs no substantial extra hardware and thus reduces the cost [49]. By modifying BSs for acting as low-power radars, the future Ultra Dense Network (UDN) having a large number of cooperative micro BSs can be exploited as the urban air defense system, which provides early warning of the incoming threats.

3) Radar-assisted low-probability-of-intercept (LPI) communication

The need for covert communication has emerged in many defense-related applications, where sensitive information such as the locations of critical facilities should be protected during transmission. The probability of intercept is thus defined as a key performance metric for secrecy communications. Conventionally, LPI is achieved by frequency/time hopping or spread-spectrum methods, which require vast time and frequency resources [50], [51]. From a CRSS viewpoint, however, a more cost-efficient approach would be to embed the communication signal into the radar echo to mask the data transmission [14], [52], [53].

A general model for the above scenario is composed of an RF tag/transponder within a collection of scattered targets and a radar transceiver. The radar firstly emits a probing waveform, which is captured by the RF tag. The tag then remodulates the radar signal with communication information and sends it back to the radar. The signal received is naturally embedded in the reflected radar returns [14]. The communication waveform should be appropriately designed by controlling its transmit power and the correlation/similarity with the radar waveform. As such, the communication signal can be hard to recognize at an adversary's side, since it is hidden among the random clutter and echoes. Nevertheless, it can be easily decoded at the radar by exploiting some *a priori* knowledge [52]. Accordingly, a number of performance trade-offs among radar sensing, communication rate and information confidentiality can be achieved by well-designed waveforms and advanced signal processing techniques.

4) Passive radar

From a broader viewpoint, passive radar, which exploits scattered signals gleaned from non-cooperative communication systems, could be classified as a special type of CRSS technology. Such illumination sources can be television signals, cellular BSs and digital video/audio broadcasting (DVB/DAB) [54]. To detect a target, the passive radar firstly receives a reference signal transmitted from a direct LoS path (usually referred to as "reference channel") from the above external TXs. In the meantime, it listens to the scattered counterpart of the same reference signal that is generated by potential targets (referred to as "surveillance channel") [55], [56]. Note that these scattered signals contain target information similarly to the case of active radars. As a consequence, the related target parameters can be estimated by computing the correlation between signals gleaned from the two channels.

The passive radar is known to be difficult to locate or be interfered, since it remains silent when detecting targets, and hence it is advantageous for covert operations. Furthermore, it requires no extra time/frequency resources, leading to a cost that is significantly lower than that of its conventional active counterparts. For this reason, it has been termed "green radar" [55]. Nonetheless, it may suffer from poor reliability due to the facts that the signal used is not specifically tailored for target detection, and that the transmit source is typically not under the control of the passive radar [55]. To further improve the detection probability while guaranteeing a satisfactory communication performance, joint waveform designs and resource allocation approaches could be developed by invoking CRSS techniques [57].

For clarity, we summarize the aforementioned application scenarios of CRSS technologies in TABLE IV.

II. Literature Review

In this section, we review recent research progress in the area of CRSS. We will first present coexistence approaches for radar and communication systems, and then present the family of the dual-functional radar-communication system designs.

A. Radar-Communication Coexistence (RCC)

1) Opportunistic spectrum access

Opportunistic spectrum access can be viewed as an extension of cognitive radio, in which the radar is regarded as the primary user (PU) of the spectrum, and the communication system plays the role of the secondary user (SU). Such methods typically require the SU to sense the spectrum, and transmit when the spectrum is unoccupied. To avoid imposing interference on the radar, the communication system has to control its power to ensure that the radar's interference-to-noise ratio (INR) does not become excessive [58]. A similar approach has been adopted in [59] for the coexistence of a rotating radar and a cellular BS. In this scenario, the mainlobe of the radar antenna array rotates periodically to search for potential targets. The BS is thus allowed to transmit only when it is in the sidelobe of the radar. Under this framework, the minimum distance between the two systems is determined given the tolerable INR level, and the communication performance is also analyzed in terms of the DL data rate.

Although easy to implement in realistic scenarios, the above approaches do not really share the spectrum. This is because the communication system can work only when the radar is not occupying the frequency and the spatial resources. Additionally, the aformentioned contributions do not easily extend to facilitate coexistence with MIMO radar. Unlike conventional radars, the MIMO radar transmits omnidirectional waveforms to search for unknown targets across the whole space, and formulates directional beams to track known targets of interest [60], [61]. Consequently, it is hard for the BS to identify the sidelobes of the MIMO radar, since the radar beampattern may change randomly along with the movement of the targets. Therefore, more powerful techniques such as transmit precoding design are required to cancel the mutual interference.

2) Interference channel estimation

Before designing a transmit precoder, channel state information on the interference channel (ICSI), i.e. the channel over which the mutual interference signals propagate, should be firstly obtained. Conventionally, this information is obtained by exploiting pilot signals sent to the radar by the communication system, where classic methods such as least-squares (LS) and minimum mean squared error (MMSE) channel estimation methods [62] could be readily applied. Nevertheless, such schemes might consume extra computational and signaling resources [63]. As another option, it was proposed in [64] to build a dedicated control center connected to both systems via wireless or backhaul links, which would carry out all the coordinations including ICSI estimation and transmit precoding design. In cases where the radar has priority, the control center would be part of the radar [63]. However, such a method would involve significant overhead. A novel channel estimation approach has been proposed in [65] by exploiting the radar probing waveform as the pilot signal, where the radar is oblivious to the operation of the communication system. Since the radar randomly changes its operational mode from searching to tracking, the BS has to firstly identify the working modes of the radar by hypothesis testing methods, and then estimate the channel.

3) Closed-form precoder design

After estimating the interference channel, the precoder can be designed at either the radar or the communication's side. Similar to zero-forcing (ZF) precoding for classic MIMO communication system, a simple idea is the so-called null-space projection (NSP) [66], which typically requires the radar to have knowledge of the ICSI. In the NSP scheme, the radar firstly obtains the right singular vectors of the interference channel matrix by singular value decomposition (SVD), and then constructs an NSP precoder relying on the vectors associated with the null space of the channel. The precoded radar signal is projected onto the null-space of the channel, so that the interference power received at the BS is strictly zero. However, such a precoder might lead to serious performance losses of the MIMO radar, for example by eroding the spatial orthogonality of the searching waveform. To cope with this issue, the authors of [67] designed a carefully adjusted threshold for the singular values of the channel matrix and then formulated a relaxed NSP precoder by the right singular vectors associated with singular values that are smaller than the threshold. By doing so, the radar performance can be improved at the cost of increasing the interference power received at the BS.

Despite the above-mentioned benefits, there are still a number of drawbacks in NSP based approaches. For instance, the interference power cannot be exactly controlled, since it is proportional to the singular values of the random channel. Additionally, since the target's response might fall into the row space of the communication channel matrix, it will be zero-forced by the NSP precoder and as a consequence, be missed by the radar. Fortunately, these disadvantages could be overcome by use of convex optimization techniques, which optimize the performance of both systems under controllable constraints [64], [68].

4) Optimization based designs

Pioneering effort on optimization based beamforming/signaling for the RCC is the work in [68], where the coexistence of a point-to-point (P2P) MIMO communication system and a Matrix-Completion MIMO (MC-MIMO) radar is considered. As a computationally efficient modification of the MIMO radar, the MC-MIMO radar typically employs a sub-sampling matrix to sample the receive signal matrix of the target echoes, and approximately recovers the target information using the matrix completion algorithm [68]. The random sub-sampling at the radar receive antennas modulates the interference channel, and enlarges its null space. This gives the opportunity to the communication system to design its precoding scheme so that it minimizes the interference caused to the radar. In [68], the covariance matrix of the communication signal and the sub-sampling matrix of the MC-MIMO radar are jointly optimized, subject to power and

capacity constraints. The corresponding optimization problem is solved via Lagrangian dual decomposition and alternating minimization methods. By taking realistic constraints into consideration, the authors further introduce signal-dependent clutter into the coexistence scenario in [64], which has to be reduced in order to maximize the effective SINR of the radar while guaranteeing the communication performance. Based on the observation that while the interference imposed by the communication system onto the radar is persistent, the interference inflicted by the radar upon the communication link is intermittent [64], the coexistence issues of a communication system and a pulsed radar were considered in [69], and the communication rate was quantified as the weighted sum of the rates with and without the radar interference (*compound rate*). The authors then formulate an optimization problem to maximize the rate subject to power and radar SINR constraints. It is worth noting that this problem can be solved in closed-form when the radar interference satisfies certain conditions.

To address the coexistence problem of the MIMO radar and the multi-user MIMO (MU-MIMO) communication system, the authors of [70] propose a robust beamforming design at the MIMO BS assuming that the ICSI between the radar and the communication system is imperfectly known. An optimization problem is formulated for maximizing the detection probability of the radar, while guaranteeing the power budget of the BS and the SINR of the DL users. An interference alignment for transmit precoding design is proposed in [71] with special emphasis on the degree of freedom (DoF), under the scenario in which multiple communication users coexist with multiple radar users. To minimize the Cramér-Rao bound (CRB) for radar target estimation in the presence of the interference arrived from a MU-MIMO communication system, a novel optimization technique based on Alternating Direction Method Of Multipliers (ADMM) has been developed in [72] for solving the non-convex problems. As a step further, a constructive interference based beamforming design has been proposed for the coexistence scenario [73], where the known DL multi-user interference (MUI) is utilized for enhancing the useful signal power. As a result, the SINR of the DL users is significantly improved compared to that of [70] given the same transmit power budget. We refer readers to [74] for more details on the topic of interference exploitation.

5) Receiver designs

We end this section by briefly reviewing the receiver design that has been proposed for coexistence of radar and communications. The aim of such a receiver is to estimate the target parameters in the presence of the communication interference, or demodulate the communication data while cancelling the radar interference. To the best of our knowledge, most of the existing research is focused on the second type, i.e., on the design of receivers for communication systems.

In [75], a spectrum sharing scenario is considered, in which a communication receiver coexists with a set of radar/sensing systems. In contrast to the cooperative scenarios discussed in the relevant literature [64], [66], [68], [75] assumes that the only information available at the communication system is that the interfering waveforms impinging from the radars fall into the subspace of a known dictionary. Given the sparse properties of both the radar interference and the communication demodulation errors, several optimization algorithms have been proposed for simultaneously estimating the radar interference, whilst demodulating the communication symbols based on compressed sensing (CS) techniques. It is shown that the associated optimization problems can be efficiently solved via non-convex factorization and conjugate gradient methods.

In a typical coexistence scenario, the communication system periodically receives radar interfering pulses having high amplitudes and short durations, which implies that a narrowband communication receiver experiences radar interference as an approximately constant-amplitude additive signal. Due to the slow variation of the radar parameters, this amplitude can be accurately estimated. Nevertheless, the phase shift of the interfering signal is sensitive to the propagation delay, thus is difficult to obtain. In [76], the authors exploit the assumption that the amplitude of the radar interference is known to the communication receiver, whereas the phase shift is unknown and uniformly distributed on $[0, 2\pi]$. With the presence of the interfering signal receiving from the radar, a pair of communication-related issues have been studied. The first one is how to formulate the optimal decision region on a given constellation based on the maximum likelihood (ML) criterion. The second one, on the other hand, is how to design self-adaptive constellations that optimize certain metrics, namely the communication rate and the symbol error rate (SER). It is observed via numerical simulations that the optimal constellation tends to a concentric hexagon shape for low-power radar interference and to an unequally-spaced pulse amplitude modulation (PAM) shape for the high-power counterpart.

B. Dual-functional Radar-Communication (DFRC) System

1) Information theory for the DFRC

It is well understood that the radar works in a way that is fundamentally different from classic communication systems. Specifically, the communication takes place between two or more cooperative transceivers. By contrast, radar systems send probing signals to uncooperative targets, and infer useful information contained in the target echoes. To some degree, the process of radar target probing may be deemed as similar to the communication channel estimation, with the probing waveforms acting as the pilot symbols. For designing a DFRC system, one can unify radar and communication principles by invoking information theory, which may reveal fundamental performance bounds of the dual-functional systems [77].

In a communication system, the transmitted symbols are drawn from a discrete constellation that is known to both TX and RX, which enables the use of *bit rate* as a performance metric for the communication. By contrast, the useful information for radar is not in the probing waveform but rather in the echo signal reflected by the target, which is however not drawn from a finite-cardinality alphabet [40]. Drawing parallels from information theory, one way to measure the radar information rate is to view each resolution unit of the radar as a "constellation point", as each unit can accommodate a distinguishable point-like target. In [78], the "channel capacity" of the radar

is defined as the number of distinguishable targets, which is the maximum information that can be contained in the echo wave.

In addition to the above definition, the authors of [77] have considered the mutual information between the radar and the target. Intuitively, the variance of the noise imposed on the echo wave represents the uncertainty of the target information, and can be measured by the entropy of the echo. From an information theoretical viewpoint, the radar cancels part of the uncertainty by estimating the target parameters, where the remaining part is lower-bounded by the Cramér-Rao Bound (CRB), which can be viewed as the minimum variance achievable of the estimated parameter [79]. In light of this methodology, [77] considers a single-antenna DFRC receiver, which can process the target echo wave and the UL communication signal simultaneously. Such a channel can be viewed as a special multi-access (MAC) channel, where the target is considered as a virtual communication user. An estimation rate is defined as the information metric for the radar in [77]. By invoking the analytical framework of the communication-only MAC channel, the trade-off between radar and communication performances is analyzed under different multi-access strategies. In [80], an integrated metric is proposed for the DFRC receiver, which is the weighted sum of the estimation and communication rates. More recently, this approach has been generalized to the multi-antenna DFRC system in [81]. While the performance bounds of the DFRC systems have been specified by the above contributions, the design of DFRC waveforms is still an open problem.

2) Temporal and spectral processing

Depending on their specific transmission strategy, radar systems can be classified into two categories, i.e. continuous-wave (CW) radar and pulsed radar [82]. CW radar continuously transmits a probing signal, while simultaneously receiving the echo reflected by the target, and hence requires high isolation between the TX and RX antennas. On the other hand, the pulsed radar periodically emits short and high-power pulses, where the transmission and the reception are operated in a time-division (TD) manner. Therefore the same antenna can be used both as TX and RX [83]. Among various probing waveforms, chirp signals, or linear frequency modulation (LFM) signals, are of interest in both categories of radars [83]. CW radar using linear or nonlinear chirp signals is also referred to as frequency modulated CW (FMCW) radar [83]. For pulsed radar, the chirp signal is exploited for improving the range resolution (by increasing the signal bandwidth) and also the maximum detectable range (by increasing the pulse duration/energy) with the aid of the pulse compression (PC) technique [84]. Furthermore, phase-coded waveforms, e.g. Barker codes, are also widely employed by the pulsed radar, where chip-by-chip phase modulation is applied for achieving desired PC outputs, including mainlobe shape, sidelobe level and Doppler tolerance, etc [84]. To the best of our knowledge, most of the state-of-the-art DFRC waveforms are tailored for pulsed radar systems, which we briefly introduce in the following.

In the early 1960s, the pioneering treatise [85] proposed to modulate communication bits onto radar pulses by the classical pulse interval modulation (PIM), which shows that one can design dual-functional waveforms by embedding useful information into radar signals. By realizing this, [86], [87] propose to modulate chirp signals with communication bit sequences, where 0 and 1 are differentiated by exploiting the quasi-orthogonality of the up and down chirp waveforms. Likewise, the pseudo-random codes can also be used both as the probing signal and the information carrier [88]. A simpler approach is proposed in [89] under a time-division framework, where the radar and the communication signals are transmitted in different time slots and thus do not interfere with each other.

In addition to the above approaches where the DFRC waveforms are designed from the ground-up, a more convenient option would be to employ the existing communication signals for target detection. In this spirit, the classic Orthogonal Frequency Division Multiplexing (OFDM) signal is considered as a promising candidate [90]. In [91], the authors proposed to transmit OFDM communication signals for vehicle detection. The impact of the random data can be eliminated by simple element-wise division between the transmitted OFDM symbols and the received echoes. In contrast to its single-carrier counterpart, the OFDM approach of [91] employs the fast Fourier transform (FFT) and the inverse FFT (IFFT) for Doppler and range processing, respectively, which obtains the Doppler and the range parameters in a decoupled manner. It is also possible to replace the sinusoidal subcarrier in the OFDM as the chirp signal [92]. Accordingly, the fractional Fourier transform (FrFT) [93], which is built upon orthogonal chirp basis, is used to process the target return.

3) Spatial processing

On top of the above temporal and spectral signal processing, it is equally important to develop spatial signal processing techniques for DFRC systems with the support of multiple antennas. While MIMO communication systems have been deployed worldwide since their invention in the 1990s [94]–[96], it should be highlighted that it was the radar scientists who first conceived the multi-antenna technology. During World War II, phased-array radar was independently invented by the American Nobel laureate Luis Alvarez [97] and the German company GEMA [98]. A typical phased-array radar transmits via each antenna the appropriately phase-shifted counterpart of a benchmark signal, and hence can electronically steer the probing beam towards any direction of interest. Nevertheless, such a transmission scheme inevitably leads to limited degrees-of-freedom (DoFs) in the waveform design, which may result in performance-loss when there are multiple targets to be detected. To address this limitation, the concept of co-located MIMO radar [2] was proposed in 2004 [99], [100], which transmits individual waveforms from each antenna. Consequently, the echoes could be re-assigned to the MIMO radar receiver by exploiting the associated waveform diversity, leading to an enlarged virtual array. By exploiting the resultant higher DoFs, the MIMO radar achieves higher detection probability and estimation accuracy, hence becomes an essential architecture for the state-of-the-art DFRC systems.

[2]There is also concept of MIMO radar with widely separated antennas, which is outside the scope of this paper.

As a key issue in multi-antenna signal processing, angle estimation have raised considerable research interests in the academia. Classic subspace based techniques, such as MUltiple SIgnal Classification (MUSIC) [101] and Estimation of Signal Parameters via Rotational Invariance Techniques (ESPRIT) [102], can be readily applied to the MIMO radar as well as the MIMO DFRC system. By contrast, data-dependent methods such as Capon [103] and Amplitude and Phase Estimation (APES) [104] algorithms are also good candidates for receive beamforming design. To exploit the merits of both Capon and APES, a novel estimator called CAPES, i.e., the combination of the two techniques, has been proposed in [105] for the MIMO radar to achieve both superior angle and amplitude estimation performances.

By relying on both the waveform diversity of the MIMO radar and the space-division multiple access (SDMA) concept of the MIMO communication, a straightforward MIMO DFRC scheme is to detect the target in the mainlobe of the radar antenna array, while transmitting useful information in the sidelobe. One can simply modulate the sidelobe level using amplitude shift keying (ASK), where different powers represent different communication symbols [106]. Similarly, classic phase shift keying (PSK) could also be applied for representing the bits as the phases of the signals received at the angle of the sidelobe [107]. Accordingly, multi-user communication can be implemented by varying the sidelobes at multiple angles. To avoid any undue performance-loss of the radar, beampattern invariance based approaches have been studied in [108], where the communication symbols are embedded by shuffling the transmitted waveforms across the antenna array. In this case, the information is embedded into the permutation matrices.

In the above methods, a communication symbol is usually embedded into either a single or several radar pulses, which results in a low data rate that is tied to the pulse repetition frequency (PRF) of the radar, hence it is limited to the order of kbps. Moreover, the sidelobe embedding schemes can only work when the communication receiver benefits from a line-of-sight (LoS) channel. This is because for a multi-path channel, the received symbol will be seriously distorted by the dispersed signals arriving from Non-LoS (NLoS) paths, where all the sidelobe and the mainlobe power may contribute. To this end, the authors of [109] proposed several beamforming designs to enable joint MIMO radar transmission and MU-MIMO communication, in which the communication signal was exploited for target detection, hence it would not affect the DL data rate. The joint beamforming matrix is optimized to approach an ideal radar beampattern, while guaranteeing the DL SINR and the power budget. To conceive the constant-modulus (CM) waveform design for DFRC systems, the recent contributions [110], [111] proposed to minimize the DL multi-user interference (MUI) subject to specific radar waveform similarity and CM constraints. An efficient branch-and-bound (BnB) algorithm has been designed for solving the non-convex optimization problem, which was shown to find the global optimum in tens of iterations.

4) DFRC system in the 5G era

Although there is a rich literature on DFRC system design, the above research mainly considers the applications in sub-6 GHz band. To address the explosive growth of wireless devices and services, the forthcoming 5G network aims at an ambitious 1000-fold increase in capacity by exploiting the large bandwidth available in the mmWave band. In the meantime, it is expected that the mmWave BS will be equipped with beneficial sensing capability, which may find employment in a variety of scenarios such as V2X communication that has been discussed in Sec. I-B. Dual-functional radar-communication in mmWave systems is a new and promising research area. Recent treatises [112], [113] propose to invoke the radar function to support vehicular sensing and communication based on the IEEE 802.11ad WLAN protocol, which operates in the 60GHz band. As the WLAN standard is typically indoor based and employs small-scale antenna arrays, it can only support short-range sensing at the order of tens of meters. To overcome these drawbacks, the large-scale antenna arrays have to be exploited, which can compensate the high path-loss imposed on mmWave signals. Moreover, the high DoFs of massive antennas make it viable to support joint sensing and communication tasks. Recent research works have shown that, by leveraging the powerful massive MIMO technique for the radar, it is possible to develop a target detector using only a single snapshot, which is robust to the unknown disturbance statistics [114].

It is noticeable that all the above advantages are obtained at the price of higher hardware cost and computational complexity, which are particularly pronounced in the case of fully digital massive MIMO systems where a large number of mmWave RF chains is needed. To mitigate those issues, the maturing hybrid analog-digital (HAD) beamforming structure is typically used in such systems [115]–[118]. HAD beamforming aims at reducing the hardware costs by connecting fewer RF chains with massive antennas via phase-shifters (PSs), which provides a balance between the hardware complexity and the system performance [119]. Note that such an idea has also emerged in radar applications. While MIMO radar outperforms the phased-array radar in many aspects such as improving the angular resolution and the parameter identifiability, its receive SINR is typically lower than that of the phased-array counterpart [120] due to the loss of the coherent processing gain. Moreover, MIMO radar suffers from higher computational overhead and implementation complexity. In view of the above, a novel radar system referred to as "phased-MIMO radar" is proposed in [120], which is a compromise between both types of radars. By partitioning the antenna array into several sub-arrays [121], the phased-MIMO radar transmits individual digital signals by each RF chain, but performs coherent analog combination at each sub-array; this is expected to strike a favorable performance tradeoff between pure analog and fully digital beamforming designs.

Given the natural connections between the HAD communication and the phased-MIMO radar, we foresee great potential in combining both two techniques in the 5G era, which would enable the development of emerging applications such as V2X and massive MIMO positioning. For clarity, we summarize the timeline of the evolution of DFRC techniques in Fig. 1.

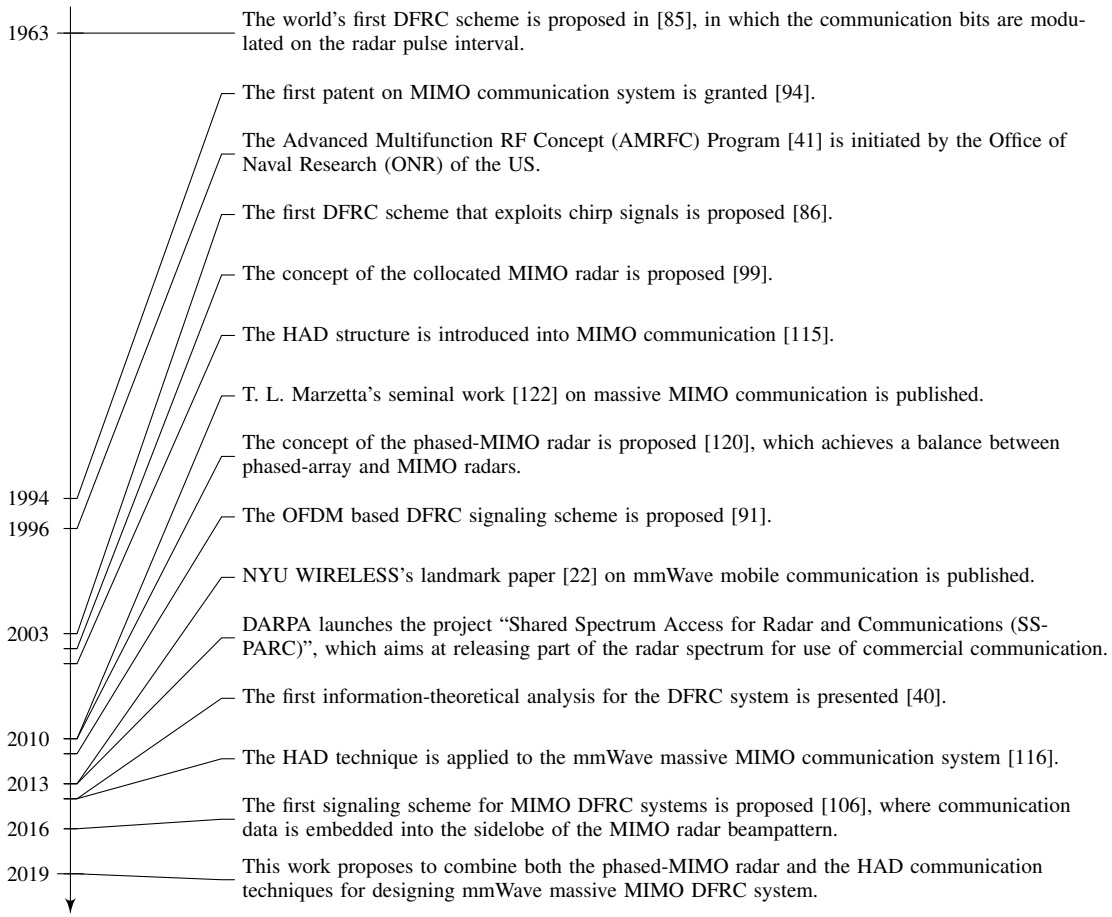

Fig. 1. Timeline of the evolution of DFRC techniques.

C. Main Contributions of Our Work

In this paper, we propose a novel architecture for a DFRC system operating in the mmWave band by combining both frameworks of the HAD communication and the phased-MIMO radar. While existing works have presented analog beamforming designs for small-scale MIMO DFRC [123], little attention has been paid to HAD based massive MIMO (mMIMO) DFRC systems, which provides additional DoFs than that of the analog-only beamforming, whilst maintaining compatibility with 5G mmWave applications. To be more specific, we consider a mMIMO mmWave BS that serves a multi-antenna UE and at the same time detects multiple targets, where part of the targets are also the scatterers fall in the communication channel. To reduce the number of RF chains, an HAD beamformer is employed for both transmission and reception at the BS. We propose a novel DFRC frame structure that complies with state-of-the-art time-division duplex (TDD) protocols, which can be split into three stages for unifying similar radar and communication operations, namely 1) radar target search and communication channel estimation, 2) radar transmit beamforming and downlink communication and 3) radar target tracking and uplink communication. In each stage, we propose joint signal processing approaches that can fulfill both target detection and communication tasks via invoking hybrid beamforming. In Stage 1, we estimate the parameters of all the potential targets and the communication channel parameters by using both DL and UL pilots. Based on the estimation results, we propose in Stage 2 a novel joint HAD transmit beamforming design that can formulate directional beams towards the angles of interest, while equalizing the communication channel. Finally, in Stage 3 we track the angular variation by simultaneously processing the echoes of the targets while decoding the UL signal transmitted from the UE. Below we boldly and crisply summarize our contributions:

- A novel mmWave mMIMO DFRC architecture that can simultaneously detect targets while communicating with the UE;
- A novel TDD frame structure capable of unifying radar and communication operations;
- A joint signal processing strategy that can search for unknown targets while estimating the communication channel;
- A joint HAD beamforming design that formulates directional beams towards targets of interest while equalizing the influence of the channel;
- A joint receiver design that can simultaneously track the variation of the targets while decoding the UL communication signals.

The remainder of this paper is organized as follows. Section III introduces the system model, Section IV proposes the basic

framework of the DFRC system, Sections V-VII consider the signal processing schemes for Stages 1, 2 and 3, respectively, Section VIII provides numerical results. Finally, Section IX concludes the paper and identifies a number of future research directions.

Notation: Unless otherwise specified, matrices are denoted by bold uppercase letters (i.e., $\mathbf{H}$), vectors are represented by bold lowercase letters (i.e., $\boldsymbol{\alpha}$), and scalars are denoted by normal font (i.e., θ). Subscripts indicate the location of the entry in the matrices or vectors (i.e., $\mathbf{F}_{RF}(i,j)$ denotes the (i,j)th entry of $\mathbf{F}_{RF}$, $\mathbf{F}_{RF}(i,:)$ and $\mathbf{F}_{RF}(:,j)$ denote the *i*th row and the *j*th column of $\mathbf{F}_{RF}$, respectively). $\mathrm{tr}(\cdot)$, $(\cdot)^T$, $(\cdot)^H$, $(\cdot)^*$ and $(\cdot)^\dagger$ stand for trace, transpose, Hermitian transpose, complex conjugate and pseudo-inverse, respectively. $\|\cdot\|$ and $\|\cdot\|_F$ denote the l_2 norm and the Frobenius norm respectively. For the sake of clarity, a full notation list is included in TABLE II.

III. System Model

We consider an N_{BS}-antenna massive MIMO DFRC BS that communicates with an N_{UE}-antenna UE while detecting multiple targets. The system operates in TDD mode, and both BS and UE are assumed to be equipped with uniform linear arrays (ULA). To reduce the number of RF chains, the BS employs a fully-connected hybrid analog-digital beamforming structure with N_{RF} RF chains, where $N_{RF} \leq N_{BS}$. Since the size of the antenna array at the UE is typically much smaller than at the BS, we assume that the UE adopts fully digital beamforming structure.

We show a generic DFRC scenario in Fig. 2, where a collection of K scatterers/radar targets are randomly distributed within the communication/sensing environment, which are yet to be detected by the BS. While all targets reflect back the echo wave to the BS, not all of them contribute to communication scattering paths between the BS and the UE. Recent literature on mmWave channel modeling has shown that the scattering model describes well the mmWave communication channel, which typically has a small number of scattered paths. We assume that only L out of K scatterers are resolvable in the communication channel, and that $L \leq N_{UE} \leq N_{BS}$. Therefore, the rank of the communication channel is L, which suggests that the channel can support up to L independent data streams to be transmitted simultaneously. For convenience, both K and L are assumed to be known to the BS.

Remark 1: From a radar perspective, not all targets are of interest. Obstacles such as trees and buildings are unwanted reflectors, and are commonly referred to as "clutter" in the radar literature. Clutter interference can be avoided by not radiating or receiving in the corresponding directions. However, some of the clutter might come from significant scatterers in the communication channel (as shown by red triangles in Fig. 1). Therefore, for the purpose of estimating the channel parameters, it might still be necessary to beamform towards those scatterers. This is distinctly different from a pure radar target detection scenario. For convenience, we will not distinguish these two types of targets, and only identify the communication paths within the collection of all the targets, which will be discussed in detail in Sec. V.

Remark 2: There might also exist targets that are neither significant scatterers in the communication channel nor of any interest to the DFRC BS. For notational convenience and following most of the seminal literature in the area [63], [66], [68], [70], [73], [105], we will not discuss such targets in detail and simply incorporate the generated interference in the noise term.

A. Radar Model

Let $\mathbf{X}_r \in \mathbb{C}^{N_{BS}\times T}$ be a probing signal matrix sent by the BS, which is composed by T snapshots along the fast-time axis. The echo wave reflected by the targets received at the BS can be expressed as

$$\mathbf{Y}_{echo} = \sum_{k=1}^{K} \alpha_k \mathbf{a}(\theta_k)\mathbf{a}^T(\theta_k)\tilde{\mathbf{X}}_k + \mathbf{Z}, \tag{1}$$

where $\mathbf{Z} \in \mathbb{C}^{N_{BS}\times T}$ represents the noise plus interference, with the variance σ_r^2, α_k denotes the complex-valued reflection coefficient of the *k*th target, θ_k is the *k*th target's azimuth angle, with $\mathbf{a}(\theta)$ being the steering vector of the transmit antenna array. In the case of ULA, the steering vector can be written in the form

$$\mathbf{a}(\theta) = \left[1, e^{j\frac{2\pi}{\lambda}d\sin(\theta)}, ..., e^{j\frac{2\pi}{\lambda}d(N_{BS}-1)\sin(\theta)}\right]^T \in \mathbb{C}^{N_{BS}\times 1}, \tag{2}$$

where d and λ denote the antenna spacing and the signal wavelength. Without loss of generality, we set $d = \lambda/2$. For notational convenience, we arrange the steering vectors into a steering matrix $\mathbf{A}(\Theta) = [\mathbf{a}(\theta_1), ..., \mathbf{a}(\theta_K)]$, $\Theta = \{\theta_1, \theta_2, ..., \theta_K\}$, and denote $[\alpha_1, ..., \alpha_K]^T$ as $\boldsymbol{\alpha}$.

Note that $\tilde{\mathbf{X}}_k$ is the delayed and Doppler-shifted counterpart of $\mathbf{X}_r$, which can be modeled as

$$\tilde{\mathbf{X}}_k = [\mathbf{X}_r \,\mathrm{diag}(\mathbf{d}_{q_k}), \mathbf{0}_{N_{BS}\times P}]\,\mathbf{J}_{p_k} \in \mathbb{C}^{N_{BS}\times(T+P)}, \tag{3}$$

where P denotes the maximum number of delayed snapshots, $\mathbf{d}_q$ characterizes the Doppler shift effect caused by the movement of the target, which is expressed as [124]

$$\mathbf{d}_q = \left[1, e^{j\frac{q}{Q}\Omega}, ..., e^{j\frac{q}{Q}\Omega(T-1)}\right]^T, \forall q = -Q, ..., -1, 1, ..., Q, \tag{4}$$

where Ω is the maximum detectable Doppler frequency, and Q is the half of the number of the Doppler bins. It follows from (4) that $\mathbf{d}_{-q} = \mathbf{d}_q^*$. Finally, $\mathbf{J}_p$ is a time-domain shifting matrix that stands for the round-trip delay of the target, which is [124]

$$\mathbf{J}_p = \begin{bmatrix} \underbrace{0\ldots0}_{p \text{ zeros}} & 1 & \ldots & 0 \\ 0\ldots0 & 0 & \ddots & \vdots \\ & & & 1 \\ \vdots & \vdots & \vdots & \\ & & & \vdots \\ 0\ldots0 & 0 & \ldots & 0 \end{bmatrix} \in \mathbb{R}^{(T+P)\times(T+P)}, \forall p = 1, ..., P, \tag{5}$$

where p is the number of the delayed snapshots. By the above notations, the *k*th target is located in the (p_k, q_k)th range-Doppler bin.

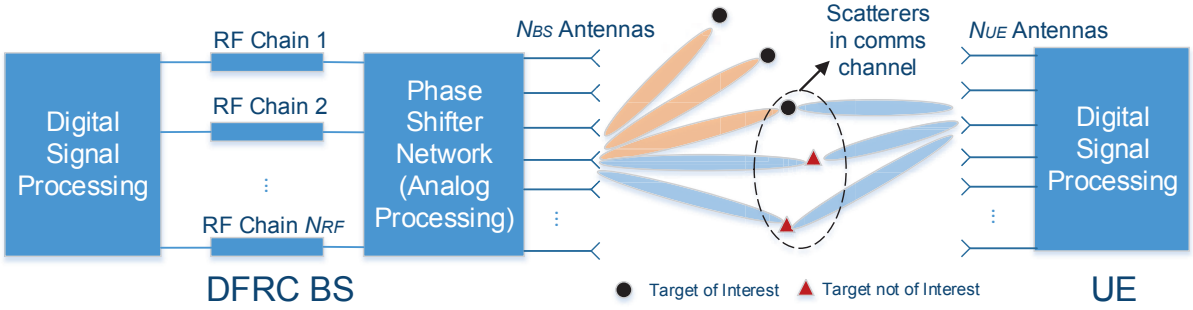

Fig. 2. MmWave dual-functional radar-communication scenario.

B. MmWave Communication Model

Let $\mathbf{X}_{DL} \in \mathbb{C}^{N_{BS} \times T}$ be a DL signal matrix sent from the BS to the UE. The received signal model at the UE can be formulated as follows by use of the extended Saleh-Valenzuela model [125], [126]:

$$\mathbf{Y}_{DL} = \sum_{l=1}^{L} \beta_l \mathbf{b}\left(\phi_l\right) \mathbf{a}^T\left(\varphi_l\right) \tilde{\mathbf{X}}_{DL,l} + \mathbf{N}_{DL}, \tag{6}$$

where $\mathbf{N}_{DL} \in \mathbb{C}^{N_{UE} \times T}$ denotes the noise with the variance of σ_{DL}^2, β_l, ϕ_l and φ_l denote the complex scattering coefficient, the DL AoA (UL AoD) and the DL AoD (UL AoA) of the lth scattering path, and

$$\mathbf{b}\left(\phi\right) = \left[1, e^{j\frac{2\pi}{\lambda}d\sin(\phi)}, ..., e^{j\frac{2\pi}{\lambda}d(N_{UE}-1)\sin(\phi)}\right]^T \in \mathbb{C}^{N_{UE} \times 1} \tag{7}$$

represents the steering vector of the UE's antenna array. Similarly to the radar model, $\tilde{\mathbf{X}}_{DL,l}$ is defined as

$$\tilde{\mathbf{X}}_{DL,l} = \left[\mathbf{X}_{DL}\, \mathrm{diag}\left(\mathbf{d}_{\tilde{q}_l}\right), \mathbf{0}_{N_{BS} \times P}\right] \mathbf{J}_{\tilde{p}_l} \in \mathbb{C}^{N_{BS} \times (T+P)}, \tag{8}$$

where $\mathbf{d}_{\tilde{q}_l}$ and $\mathbf{J}_{\tilde{p}_l}$ denote the Doppler shift vector and the temporal shifting matrix for the lth communication path, which are different from that of the radar channel. Note that the scatterers of the communication channel are also part of the targets being detected by the BS. From the perspective of the UE, the DL AoDs $\varphi_l, \forall l$ belong to the set $\Theta = \{\theta_1, ..., \theta_K\}$ of radar targets seen from the BS. We assume, without loss of generality, that $\varphi_l = \theta_l, l = 1, ..., L$, and introduce the following notations:

$$\begin{aligned} &\mathbf{B}\left(\Phi\right) = \left[\mathbf{b}\left(\phi_1\right), ..., \mathbf{b}\left(\phi_L\right)\right], \mathbf{A}\left(\Theta_1\right) = \left[\mathbf{a}\left(\theta_1\right), ..., \mathbf{a}\left(\theta_L\right)\right] \\ &\boldsymbol{\beta} = \left[\beta_1, ..., \beta_L\right]^T, \Phi = \left[\phi_1, ..., \phi_L\right], \Theta_1 = \left\{\theta_1, ..., \theta_L\right\} \subseteq \Theta. \end{aligned} \tag{9}$$

Given the reciprocity of the TDD channel, the UL communication model can be accordingly expressed as

$$\mathbf{Y}_{UL} = \sum_{l=1}^{L} \beta_l \mathbf{a}\left(\theta_l\right) \mathbf{b}^T\left(\phi_l\right) \tilde{\mathbf{X}}_{UL,l} + \mathbf{N}_{UL}, \tag{10}$$

where $\tilde{\mathbf{X}}_{UL,l}$ is defined as

$$\tilde{\mathbf{X}}_{UL,l} = \left[\mathbf{X}_{UL}\, \mathrm{diag}\left(\mathbf{d}_{\tilde{q}_l}\right), \mathbf{0}_{N_{UE} \times P}\right] \mathbf{J}_{\tilde{p}_l} \in \mathbb{C}^{N_{UE} \times (T+P)}, \tag{11}$$

with $\mathbf{X}_{UL}$ being the UL communication signal, and finally $\mathbf{N}_{UL}$ represents the noise having the variance of σ_{UL}^2. Note that for each path, time-delay and Doppler parameters remain the same despite that AoAs and AoDs are exchanged.

It can be observed in the above that the mmWave communication channel has an intrinsic geometric structure, which makes it equivalent to a bi-static radar channel [127], where the radar's TX and RX antennas are widely separated instead of being collocated as in the mono-static case of (1). Accordingly, the scatterers act as known or unknown radar targets, depending on whether the channel has been estimated. Note that such equivalences do not hold for channels modeled by stochastic distributions, e.g., Rayleigh distribution, which contain little information about the geometric environment over which the communication takes place.

IV. The Dual-functional Radar-Communication Framework

We further reveal some important insights by taking a closer look at both the radar and the communication models.

Remark 3: The aim of the communication is to decode data from the noisy signal under the knowledge of the channel state information. On the other hand, the radar acquires the geometric information of targets by sending a known probing signal. This indicates that, radar target detection is more similar to the channel estimation process rather than to the data communication itself.

Remark 4: Radar detection can also be viewed as a special communication scenario, where the targets unwillingly transmit their geometric information to the radar. Therefore, the radar targets may act as virtual communication users that communicate with the radar in an uncooperative manner.

Inspired by the above remarks, we propose the following mmWave DFRC framework, which aims for unifying radar and communication operations by joint signal processing, and can be generally split into the following three stages:

1) Radar target search and communication channel estimation

When the radar has no *a priori* knowledge about targets, the initial step is to search for potential targets in the whole space. Similarly, when no channel information is available at the communication system, the CSI has to be estimated before any useful information can be decoded at the receiver. Note that both operations require a signal with beneficial auto- and cross-correlation properties in order to extract the target parameters or the scattering characteristics of the channel.

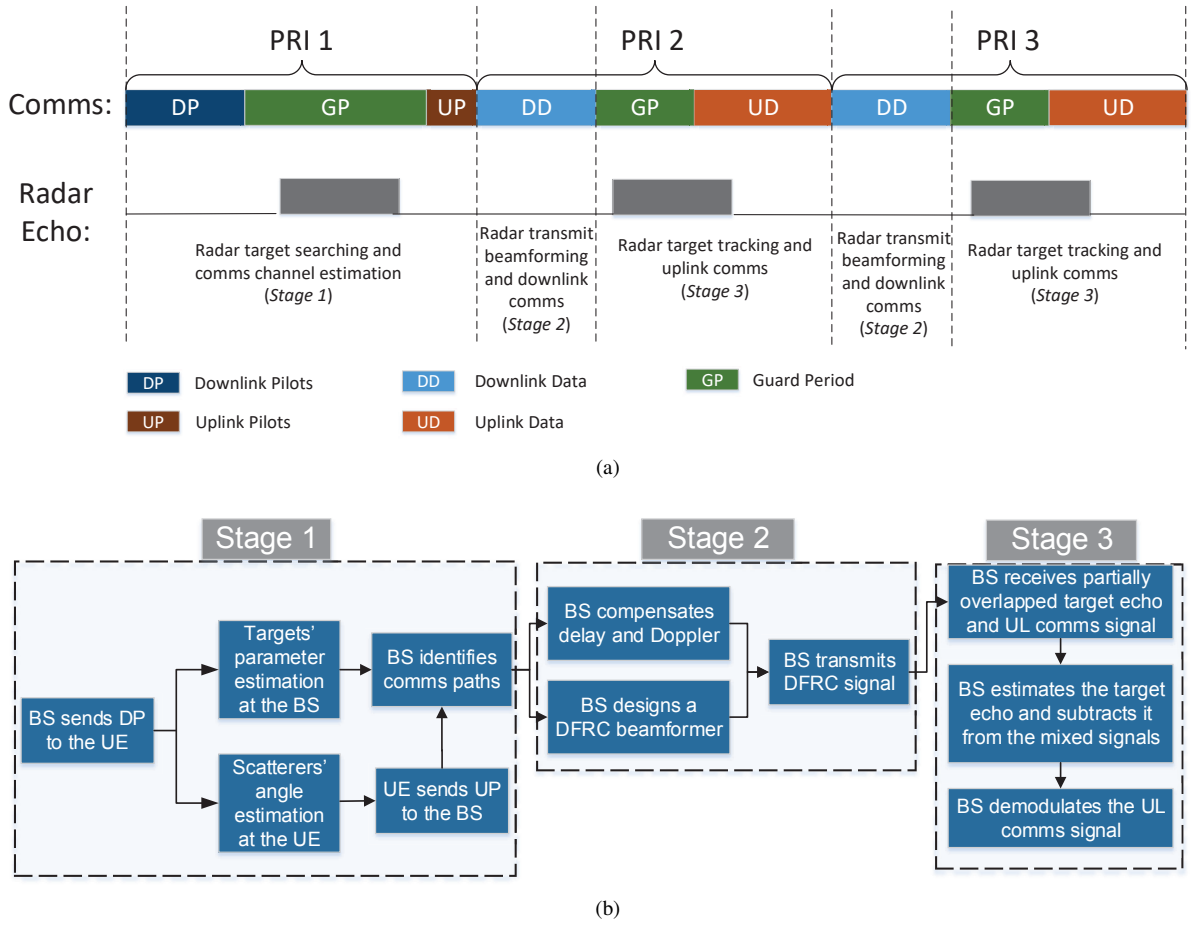

Fig. 3. (a) Frame structure of the DFRC system; (b) Signal processing flow chart.

Hence, it is natural to combine the two operations into a joint process. More specifically, in our case, the BS first sends omnidirectional DL pilots (DP), and then estimates the K AoAs in Θ as well as the associated range and Doppler parameters of all K targets. The UE also receives the probing waveform through L scattering paths, based on which it estimates L AoDs in Φ, and sends back UL pilots (UP) to the BS. By exploiting the reciprocity of the DL and the UL channels, the BS is able to identify those targets which also play the role of scatterers in the communication link, and will further estimate the Doppler and delay parameters of the corresponding communication paths. We propose a joint solution for this operation in Sec. V.

2) Radar transmit beamforming and downlink communication

After the first stage, the BS will have the estimates of $\theta_k, p_k, q_k, \forall k$ for all the targets. Nevertheless, the estimates of $\phi_l, \forall l$ are only available at the UE. The BS then formulates directional DL beams towards the angles of the targets of interest by designing a joint sensing-communication beamformer, and obtains more accurate observations. In the meantime, the BS pre-equalizes the communication channel effects via the joint beamformer designed. As such, the data can be correctly decoded at the UE. We propose and detail a joint solution for this operation in Sec. VI.

3) Radar target tracking and uplink communication

After Stage 2, the BS may receive both the target echoes and the UL signals, based on which it tracks the variation of target parameters while decoding the UL data transmitted from the UE. As we have discussed above, the targets can be viewed as virtual UEs that passively transmit their geometric parameters to the BS by reflecting the probing signal. In this spirit, we design sophisticated receive signal processing approaches to jointly fulfill both requirements, i.e., target parameter estimation and data decoding. We propose and detail a joint solution for this operation in Sec. VII.

As shown in Fig. 3(a)-(b), a specifically tailored frame structure is designed to coordinate the above DFRC operations based on a typical TDD protocol. In Stage 1, the BS transmits omnidirectional waveforms to search for targets and to estimate the communication channel, and then receives both the echoes from the targets and the UP from the UE. Since all the targets/scatterers are distributed in between the BS and the UE, and that the echoes are reflected instantaneously after hitting the targets, the round-trip from the BS to the targets/scatterers is typically shorter than that from the BS to the UE given the processing delay of the UL communication. For this reason, we assume that the target echoes are always received ahead of the UL transmission. It is worth noting that

a guard period[3] (GP) is required between DP and UP to avoid the interference between UP and target echoes [128]. The GP should be sufficiently long to cover the longest round-trip delay plus the length of the DP, so that the collision between echoes and UP can be avoided. In Stage 2, the BS transmits DL data while formulating directional beams towards all the directions in Θ and compensating the Doppler shifts and time delays, based on the measurements in Stage 1. In Stage 3, the BS receives both the echoes and the UL data, based on which it tracks the variation of the targets while decoding the UL information. Here we reserve a shorter GP between DL and UL operations to guarantee a high UL data rate, in which case the collision between the target echoes and the UL data is inevitable. To this end, we propose a successive interference cancellation (SIC) approach [129] at Stage 3 to mitigate the interference from the targets, which will be discussed in Sec. VII. It can be noted from above that the BS indeed acts as a pulsing radar that repeatedly transmits pulses and receives both echoes and UL signals. Following the standard radar literature, we term a transmit-receive cycle as a *pulse repetition interval (PRI)*.

In what follows, we will design signal processing strategies for the above three stages, respectively.

V. Stage 1: Radar Target Search and Communication Channel Estimation

In this section, we first introduce a novel pilot signal generation method for the purpose of joint target search and CSI acquisition, and then propose parameter estimation approaches at both the BS and the UE.

A. Pilot Signal Generation Using Hybrid Structure

Given a DP signal matrix $\mathbf{S}_{DP} \in \mathbb{C}^{N_{BS} \times T_P}$ with length T_P ($N_{BS} \leq T_P$), it is well-known in the field of channel estimation that the optimal performance can be achieved if its covariance matrix satisfies

$$\mathbf{R}_s = \frac{1}{T_P}\mathbf{S}_{DP}\mathbf{S}_{DP}^H = \frac{P_T}{N_{BS}}\mathbf{I}_{N_{BS}}, \tag{12}$$

where P_T is the total transmit power. It can be seen from above that the optimal pilot signal transmitted on each antenna should be spatially orthogonal. Similar investigations in the MIMO radar literature have also revealed that, the CRB of target parameter estimation can be minimized by the use of orthogonal waveforms [61], in which case the spatial beampattern can be written as

$$d\left(\theta\right) = \mathbf{a}^T\left(\theta\right)\mathbf{R}_s\mathbf{a}^*\left(\theta\right) = P_T, \ \ \forall\theta, \tag{13}$$

which is an omnidirectional beampattern. Naturally, such a beampattern transmits equivalent power at each angle, and will hence search for targets over the whole angular domain.

At a first glance, it seems that any orthogonal waveform can be used for both radar target search and channel estimation. Nevertheless, there are still some radar-specific requirements that the probing waveform should satisfy. For instance, waveforms having large time-bandwidth product (TBP) are preferred by the radar, as it offers performance improvement in both the range resolution and the maximum detectable range. To this end, we propose to employ orthogonal linear frequency modulation (LFM) signals, which are commonly used MIMO radar waveforms. According to [130], the signal transmitted at the n-th antenna at time slot t, i.e., the (n,t)th entry of a orthogonal LFM waveform matrix, can be defined as

$$\mathbf{S}_{DP}\left(n,t\right) = \sqrt{\frac{P_T}{N_{BS}}}\exp\left(\frac{j2\pi n\left(t-1\right)}{T_P}\right)\exp\left(\frac{j\pi(t-1)^2}{T_P}\right). \tag{14}$$

We see that in (14), each antenna is assigned a linear chirp waveform associated with the same slope but different start frequencies, which could be essentially viewed as OFDM-like chirp waveforms as illustrated in Fig. 4. It can be readily proven that (14) satisfies the orthogonality property (12). Next, we consider to generate such a waveform matrix by invoking the HAD array. Let us denote the baseband signal matrix by $\mathbf{S}_{BB} \in \mathbb{C}^{N_{RF} \times T_P}$, and the analog precoding matrix with unit-modulus entries by $\mathbf{F}_{RF} \in \mathbb{C}^{N_{BS} \times N_{RF}}$. The problem is to design both $\mathbf{F}_{RF}$ and $\mathbf{S}_{BB}$, such that

$$\mathbf{F}_{RF}\mathbf{S}_{BB} = \mathbf{S}_{DP}. \tag{15}$$

Due to the non-convex unit-modulus constraints imposed on $\mathbf{F}_{RF}$, it is difficult to solve the above equation directly. We therefore propose a construction method in the following.

For the signal transmitted on the nth antenna, note that as per (14), the following equation holds true for any adjacent time-slots

$$\frac{\mathbf{S}_{DP}\left(n,t+1\right)}{\mathbf{S}_{DP}\left(n,t\right)} = \exp\left(\frac{j2\pi n}{T_P}\right)\exp\left(\frac{j\pi\left(2t-1\right)}{T_P}\right). \tag{16}$$

By introducing the notation of

$$u_n = \exp\left(\frac{j2\pi n}{T_P}\right), v_t = \exp\left(\frac{j\pi\left(2t-1\right)}{T_P}\right), \tag{17}$$

$$\mathbf{u} = \left[u_1, u_2, ..., u_{N_{BS}}\right]^T, \tag{18}$$

it follows that

$$\mathbf{S}_{DP}\left(:,t+1\right) = \mathrm{diag}\left(\mathbf{u}\right)\mathbf{S}_{DP}\left(:,t\right)v_t, \forall t, \tag{19}$$

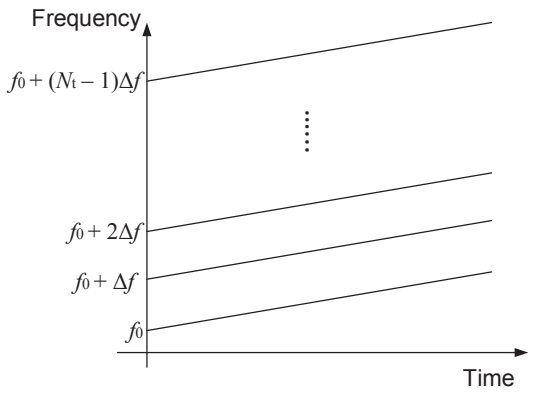

Fig. 4. Orthogonal chirp waveforms with the same slope but different start frequencies.

[3]Note that the GP is typically used in TDD protocols such as TDD-LTE.

where $\mathbf{S}_{DP}(:,t)$ denotes the tth column of $\mathbf{S}_{DP}$.

In order to generate $\mathbf{S}_{DP}$, we consider a simple strategy where the analog beamforming matrix changes on a time-slot basis [4], in which case the following two equations should be satisfied

$$\mathbf{F}_{RF}^{1}\mathbf{S}_{BB}(:,1)=\mathbf{S}_{DP}(:,1), \tag{20a}$$
$$\mathbf{F}_{RF}^{t+1}\mathbf{S}_{BB}(:,t+1)=\mathrm{diag}(\mathbf{u})\,\mathbf{F}_{RF}^{t}\mathbf{S}_{BB}(:,t)\,v_t, \tag{20b}$$

where $\mathbf{F}_{RF}^{t}$ denotes the analog beamforming matrix at the tth time-slot. Therefore, it is sufficient to let

$$\mathbf{F}_{RF}^{t+1}=\mathrm{diag}(\mathbf{u})\,\mathbf{F}_{RF}^{t},\forall t, \tag{21a}$$
$$\mathbf{S}_{BB}(:,t+1)=\mathbf{S}_{BB}(:,t)\,v_t,\forall t. \tag{21b}$$

Furthermore, noting that $\mathbf{S}_{DP}(:,1)=\sqrt{P_T/N_{BS}}\mathbf{1}_{N_{BS}}$, we can simply choose

$$\mathbf{F}_{RF}^{1}=\mathbf{1}_{N_{BS}}\mathbf{1}_{N_{RF}}^{T},\mathbf{S}_{BB}(:,1)=\sqrt{\frac{P}{N_{RF}^{2}N_{BS}}}\mathbf{1}_{N_{RF}},\forall t, \tag{22}$$

where $\mathbf{1}_N$ denotes the $N\times 1$ all-one vector. By the above method, the analog beamforming matrix and the baseband signal can be generated at each time-slot in a recursive manner. One can thus generate the LFM waveform in (14) for target search and channel estimation.

B. Parameter Estimation

After transmitting the waveform $\mathbf{S}_{DP}$ using the HAD architecture, the BS receives the signals reflected from the targets, which can be expressed as

$$\mathbf{Y}_{echo}=\sum_{k=1}^{K}\alpha_k\mathbf{a}(\theta_k)\mathbf{a}^{T}(\theta_k)\,\tilde{\mathbf{S}}_{DP,k}+\mathbf{Z}, \tag{23}$$

where

$$\tilde{\mathbf{S}}_{DP,k}=[\mathbf{S}_{DP}\,\mathrm{diag}(\mathbf{d}_{q_k}),\mathbf{0}_{N_{BS}\times P}]\,\mathbf{J}_{p_k}. \tag{24}$$

Then, the signal after analog combination can be accordingly expressed by

$$\begin{aligned}\tilde{\mathbf{Y}}_{echo}&=\sum_{k=1}^{K}\alpha_k\mathbf{W}_{RF}\mathbf{a}(\theta_k)\mathbf{a}^{T}(\theta_k)\,\tilde{\mathbf{S}}_{DP,k}+\mathbf{W}_{RF}\mathbf{Z}\\&=\sum_{k=1}^{K}\alpha_k\tilde{\mathbf{a}}(\theta_k)\mathbf{a}^{T}(\theta_k)\,\tilde{\mathbf{S}}_{DP,k}+\tilde{\mathbf{Z}},\end{aligned} \tag{25}$$

where $\mathbf{W}_{RF}\in\mathbb{C}^{N_{RF}\times N_{BS}}$ is the analog combination matrix having unit-modulus entries, $\tilde{\mathbf{a}}(\theta)=\mathbf{W}_{RF}\mathbf{a}(\theta)\in\mathbb{C}^{N_{RF}\times 1}$ is the equivalent receive steering vector, and $\tilde{\mathbf{Z}}=\mathbf{W}_{RF}\mathbf{Z}$. Since no *a priori* knowledge about the AoAs is available at this stage, there is no preference on the choice of the analog combiner. To this end, we assume that each entry of $\mathbf{W}_{RF}$ is randomly drawn from the unit circle. In what follows, we firstly estimate the angles of the targets, then the Doppler and the delay parameters, and finally the reflection coefficients.

[4]Built upon GaAs FET or PIN diode based RF switches, the state-of-the-art digital phase shifter could be tuned within several nanoseconds [131].

Remark 5: We note here that by the above analog combination, the equivalent receive array $\tilde{\mathbf{a}}(\theta)$ is indeed different from the transmit array $\mathbf{a}(\theta)$. As a result, the enlarged virtual array of the MIMO radar can still be formulated.

1) Angle estimation

To estimate the angles, we invoke the classic MUltiple SIgnal Classification (MUSIC) algorithm, which is known to have high angle resolution [132]. Let $\tilde{\mathbf{A}}(\Theta)=[\tilde{\mathbf{a}}(\theta_1),...,\tilde{\mathbf{a}}(\theta_K)]$. The eq. (25) can be equivalently recast as

$$\tilde{\mathbf{Y}}_{echo}=\tilde{\mathbf{A}}(\Theta)\,\mathrm{diag}(\boldsymbol{\alpha})\begin{bmatrix}\mathbf{a}^{T}(\theta_1)\,\tilde{\mathbf{S}}_{DP,1}\\\cdots\\\mathbf{a}^{T}(\theta_K)\,\tilde{\mathbf{S}}_{DP,k}\end{bmatrix}+\tilde{\mathbf{Z}}. \tag{26}$$

Noting the fact that $\frac{1}{N_{BS}}\mathbf{W}_{RF}\mathbf{W}_{RF}^{H}\approx\mathbf{I}_{N_{RF}}$ when N_{BS} is sufficiently large, the covariance matrix of (26) is given by

$$\begin{aligned}\mathbf{R}_{\tilde{Y}}&=\frac{1}{T_P}\tilde{\mathbf{Y}}_{echo}\tilde{\mathbf{Y}}_{echo}^{H}=\frac{P_T}{N_{BS}}\tilde{\mathbf{A}}(\Theta)\,\mathbf{R}_{\tilde{S}}\tilde{\mathbf{A}}^{H}(\Theta)+\frac{1}{T_P}\tilde{\mathbf{Z}}\tilde{\mathbf{Z}}^{H}\\&=\frac{P_T}{N_{BS}}\tilde{\mathbf{A}}(\Theta)\,\mathbf{R}_{\tilde{S}}\tilde{\mathbf{A}}^{H}(\Theta)+\sigma_r^{2}\mathbf{W}_{RF}\mathbf{W}_{RF}^{H}\\&\approx\frac{P_T}{N_{BS}}\tilde{\mathbf{A}}(\Theta)\,\mathbf{R}_{\tilde{S}}\tilde{\mathbf{A}}^{H}(\Theta)+\sigma_r^{2}N_{BS}\mathbf{I}_{N_{RF}},\end{aligned} \tag{27}$$

where

$$\mathbf{R}_{\tilde{S}}=\frac{1}{T_P+P}\,\mathrm{diag}(\boldsymbol{\alpha})\begin{bmatrix}\mathbf{a}^{T}(\theta_1)\,\tilde{\mathbf{S}}_{DP,1}\\\cdots\\\mathbf{a}^{T}(\theta_K)\,\tilde{\mathbf{S}}_{DP,k}\end{bmatrix}\begin{bmatrix}\mathbf{a}^{T}(\theta_1)\,\tilde{\mathbf{S}}_{DP,1}\\\cdots\\\mathbf{a}^{T}(\theta_K)\,\tilde{\mathbf{S}}_{DP,k}\end{bmatrix}^{H}\mathrm{diag}(\boldsymbol{\alpha}^{*}). \tag{28}$$

Following the standard MUSIC algorithm, the eigenvalue decomposition of (27) is formulated as

$$\mathbf{R}_{\tilde{Y}}=[\mathbf{U}_s,\mathbf{U}_n]\begin{bmatrix}\boldsymbol{\Sigma}_s&\\&\boldsymbol{\Sigma}_n\end{bmatrix}\begin{bmatrix}\mathbf{U}_s^{H}\\\mathbf{U}_n^{H}\end{bmatrix}, \tag{29}$$

where $\mathbf{U}_s\in\mathbb{C}^{N_{RF}\times K}$ and $\mathbf{U}_n\in\mathbb{C}^{N_{RF}\times(N_{RF}-K)}$ contain eigenvectors, which span the signal and the noise subspaces, respectively. It then follows that

$$\mathrm{span}\left(\tilde{\mathbf{A}}(\Theta)\right)=\mathrm{span}(\mathbf{U}_s),\mathrm{span}\left(\tilde{\mathbf{A}}(\Theta)\right)\perp\mathrm{span}(\mathbf{U}_n), \tag{30}$$

which suggests that $\tilde{\mathbf{a}}(\theta_k),\forall k$ are orthogonal to $\mathbf{U}_n$. The MUSIC spectrum can be thus formulated as

$$P_{\text{MUSIC}}(\theta)=\frac{1}{\tilde{\mathbf{a}}^{H}(\theta)\,\mathbf{U}_n\mathbf{U}_n^{H}\tilde{\mathbf{a}}(\theta)}. \tag{31}$$

By finding the K largest peaks of (31), we can readily locate the AoAs of the K targets.

Remark 6: When the BS does not know the exact number of targets, one can simply estimate this number by exploiting the fact that the eigenvalues associated with the signal subspace are much higher than those associated with the noise subspace. By arranging the eigenvalues in a descending order, there will be a sufficiently high difference between the Kth and the $(K+1)$th eigenvalues, which can be identified with a high confidence. By doing so, the number of targets K can be accordingly estimated.

2) Delay and Doppler estimation

The next step is to estimate Delay and Doppler parameters, i.e., q_k and p_k, that are associated with each AoA. By denoting the estimated AoAs as $\hat{\theta}_k, \forall k$, we first vectorize the reference signal in each range-Doppler bin as

$$\mathbf{g}_{k,q,p} = \text{vec}\left(\tilde{\mathbf{a}}\left(\hat{\theta}_k\right)\mathbf{a}^T\left(\hat{\theta}_k\right)\left[\mathbf{S}_{DP}\,\text{diag}\left(\mathbf{d}_q\right),\mathbf{0}_{N_{BS}\times P}\right]\mathbf{J}_p\right), \forall k,q,p, \tag{32}$$

where $\mathbf{d}_q$ and $\mathbf{J}_p$ are defined by (4) and (5), which represent the qth Doppler bin and the pth range bin, respectively. Let us denote $\tilde{\mathbf{y}}_{echo} = \text{vec}\left(\tilde{\mathbf{Y}}_{echo}\right), \tilde{\mathbf{z}} = \text{vec}\left(\tilde{\mathbf{Z}}\right)$. Note that if $\theta_k = \hat{\theta}_k$, i.e., the angles of the targets are perfectly estimated, eq. (25) can be equivalently written as

$$\tilde{\mathbf{y}}_{echo} = \left[\mathbf{g}_{1,q_1,p_1}, \mathbf{g}_{2,q_2,p_2}, \dots \mathbf{g}_{K,q_K,p_K}\right]\boldsymbol{\alpha} + \tilde{\mathbf{z}} \triangleq \mathbf{G}\boldsymbol{\alpha} + \tilde{\mathbf{z}}. \tag{33}$$

By noting the fact that

$$\left|\mathbf{g}_{k,q,p}^H \mathbf{g}_{k,q',p'}\right| \ll \left|\mathbf{g}_{k,q,p}^H \mathbf{g}_{k,q,p}\right|, \forall p, q \neq p', q', \tag{34}$$

we propose a simple matched-filtering (MF) algorithm [124] to estimate the Doppler and range parameters as follows [5].

Algorithm 1 MF Algorithm for Delay and Doppler Estimation

Input: $\tilde{\mathbf{y}}_{echo}$, $\hat{\theta}_k, \forall k$
Output: The estimated parameters $\hat{p}_k, \hat{q}_k$ for each target
1. Initialize $k = 1$.
while $k \leq K$ **do**
2. $\hat{p}_k, \hat{q}_k = \arg\max_{p,q} \left|\tilde{\mathbf{y}}_{echo}^H \mathbf{g}_{k,q,p}\right|$.
3. $\tilde{\mathbf{y}}_{echo} = \tilde{\mathbf{y}}_{echo} - \frac{\tilde{\mathbf{y}}_{echo}^H \mathbf{g}_{k,\hat{p}_k,\hat{q}_k}}{\mathbf{g}_{k,\hat{p}_k,\hat{q}_k}^H \mathbf{g}_{k,\hat{p}_k,\hat{q}_k}} \cdot \mathbf{g}_{k,\hat{p}_k,\hat{q}_k}$.
4. $k = k + 1$.
end while

Note that in Algorithm 1, line 2 exploits the fact that the reference signal in the matched range-Doppler bin will yield the maximum output with high probability, after which the estimated signal component will be subtracted from $\tilde{\mathbf{y}}_{echo}$ in line 3 to avoid interfering the estimation of other targets. By the above procedure, we can readily obtain the estimates of all the delay and Doppler parameters.

3) Reflection coefficient estimation

Finally, we estimate α_k associated with each target. Since the estimated parameters $\hat{\theta}_k, \hat{p}_k$ and $\hat{q}_k$ are now available, we employ the Angle and Phase EStimation (APES) algorithm of [104], [105] to obtain an estimated α_k with superior accuracy. Given the estimated parameters for each target, the APES technique aims at solving the following optimization problem [105]

$$\begin{aligned} &\min_{\boldsymbol{\lambda}_k, \alpha_k} \left\|\boldsymbol{\lambda}_k^H \tilde{\mathbf{Y}}_{echo} - \alpha_k \mathbf{a}^T\left(\hat{\theta}_k\right)\hat{\mathbf{S}}_{DP,k}\right\|^2 \\ &s.t. \quad \boldsymbol{\lambda}_k^H \tilde{\mathbf{a}}\left(\hat{\theta}_k\right) = 1, \end{aligned} \tag{35}$$

[5]Note that for the case of insignificant Doppler shift, we can readily estimate the Doppler frequency by classic Fourier analysis for multiple pulses in the slow-time domain.

where $\boldsymbol{\lambda}_k \in \mathbb{C}^{N_{RF}\times 1}$ is the weighting vector, and $\hat{\mathbf{S}}_k$ is defined as the recovered echo reflected by the kth target based on the estimated range and Doppler parameters, which is

$$\hat{\mathbf{S}}_{DP,k} = \left[\mathbf{S}_{DP}\,\text{diag}\left(\mathbf{d}_{\hat{q}_k}\right),\mathbf{0}_{N_{BS}\times P}\right]\mathbf{J}_{\hat{p}_k}. \tag{36}$$

The intuition behind (35) is that by applying the beamforming vector $\boldsymbol{\lambda}_k$, the distance between the output signal and the echo of the kth target is minimized. In other words, the power of other targets' echoes is expected to be canceled under the constraint that the power of the kth echo being fixed as 1. To solve (35), note that for a given $\boldsymbol{\lambda}_k$, the problem degrades to a scalar least-squares (LS) optimization in terms of α_k, where the optimal α_k can be given in closed-form as

$$\hat{\alpha}_k = \frac{\boldsymbol{\lambda}_k^H \tilde{\mathbf{Y}}_{echo} \hat{\mathbf{S}}_{DP,k}^H \mathbf{a}^*\left(\hat{\theta}_k\right)}{\mathbf{a}^T\left(\hat{\theta}_k\right)\hat{\mathbf{S}}_{DP,k}\hat{\mathbf{S}}_{DP,k}^H \mathbf{a}^*\left(\hat{\theta}_k\right)}. \tag{37}$$

By substituting (37) into (35), the optimization problem is recast as

$$\min_{\boldsymbol{\lambda}_k} \boldsymbol{\lambda}_k^H \hat{\mathbf{Q}} \boldsymbol{\lambda}_k \;\; s.t. \;\; \boldsymbol{\lambda}_k^H \tilde{\mathbf{a}}\left(\hat{\theta}_k\right) = 1, \tag{38}$$

where

$$\hat{\mathbf{Q}} = \frac{\tilde{\mathbf{Y}}_{echo}\tilde{\mathbf{Y}}_{echo}^H}{T_P + P} - \frac{\tilde{\mathbf{Y}}_{echo}\hat{\mathbf{S}}_{DP,k}^H \mathbf{a}^*\left(\hat{\theta}_k\right)\mathbf{a}^T\left(\hat{\theta}_k\right)\hat{\mathbf{S}}_{DP,k}\tilde{\mathbf{Y}}_{echo}^H}{\left(T_P + P\right)\mathbf{a}^T\left(\hat{\theta}_k\right)\hat{\mathbf{S}}_{DP,k}\hat{\mathbf{S}}_{DP,k}^H \mathbf{a}^*\left(\hat{\theta}_k\right)}. \tag{39}$$

It can be easily observed that (38) is nothing but a Capon beamforming problem, whose globally optimal solution is known as [103]

$$\boldsymbol{\lambda}_k = \frac{\hat{\mathbf{Q}}^{-1}\tilde{\mathbf{a}}\left(\hat{\theta}_k\right)}{\tilde{\mathbf{a}}^H\left(\hat{\theta}_k\right)\hat{\mathbf{Q}}^{-1}\tilde{\mathbf{a}}\left(\hat{\theta}_k\right)}. \tag{40}$$

By substituting (40) into (37), we can readily obtain the estimated coefficient $\hat{\alpha}_k$ as

$$\hat{\alpha}_k = \frac{\tilde{\mathbf{a}}^H\left(\hat{\theta}_k\right)\hat{\mathbf{Q}}^{-1}\tilde{\mathbf{Y}}_{echo}\hat{\mathbf{S}}_{DP,k}^H \mathbf{a}^*\left(\hat{\theta}_k\right)}{\tilde{\mathbf{a}}^H\left(\hat{\theta}_k\right)\hat{\mathbf{Q}}^{-1}\tilde{\mathbf{a}}\left(\hat{\theta}_k\right)\mathbf{a}^T\left(\hat{\theta}_k\right)\hat{\mathbf{S}}_{DP,k}\hat{\mathbf{S}}_{DP,k}^H \mathbf{a}^*\left(\hat{\theta}_k\right)}. \tag{41}$$

C. Identifying Communication Channel Paths from Targets

While the BS has the knowledge of all the AoAs of targets, it still remains for us to distinguish which targets contribute to the scattering paths in the communication channel. In other words, the BS has to separate Θ_1 from $\Theta_2 \triangleq \Theta \backslash \Theta_1$, where Θ and Θ_1 are defined in (9). In addition, we still have to estimate range-Doppler parameters $\tilde{p}_l, \tilde{q}_l$ and the scattering coefficient β_l for each scattering path, as these are not equivalent to those estimated from the reflected echoes (23).

Before doing so, the UE should firstly estimate part of the target parameters from the received downlink pilot signal, which is given by

$$\mathbf{Y}_{DL} = \sum_{l=1}^{L} \beta_l \mathbf{b}\left(\phi_l\right)\mathbf{a}^T\left(\theta_l\right)\tilde{\mathbf{S}}_{DP,l} + \mathbf{N}_{DL}, \tag{42}$$

where $\tilde{\mathbf{S}}_{DP,l}$ is similarly defined as in (24) with the corresponding range and Doppler parameters $\tilde{p}_l, \tilde{q}_l$. Given the limited computational capability of the UE, only the angle parameters, i.e., $\phi_l, \forall l$, are estimated via the MUSIC algorithm for each scattering path. Accordingly, range and Doppler parameters will be estimated at the BS via receiving the uplink pilots.

With the estimated angles $\hat{\Phi} = \left\{\hat{\phi}_1, \hat{\phi}_2, \ldots, \hat{\phi}_L\right\}$ at hand, the UE formulates the following transmit beamformer

$$\mathbf{F}_{UE} = \mathbf{B}^* \left(\hat{\Phi}\right) \left(\mathbf{B}^T \left(\hat{\Phi}\right) \mathbf{B}^* \left(\hat{\Phi}\right)\right)^{-1} \in \mathbb{C}^{N_{UE} \times L}, \quad (43)$$

where $\mathbf{B}\left(\hat{\Phi}\right) = \left[\mathbf{b}\left(\hat{\phi}_1\right), \mathbf{b}\left(\hat{\phi}_2\right), \ldots, \mathbf{b}\left(\hat{\phi}_L\right)\right]$. The beamformer (43) is designed for zero-forcing the steering matrix $\mathbf{B}(\Phi)$ as defined in (9). Following the frame structure proposed in Sec. IV, the UE then sends the UP to the BS by using $\mathbf{F}_{UE}$. Without loss of generality, we assume that the UP is still composed by orthogonal LFM waveforms, which is defined similarly to (14) as

$$\mathbf{S}_{UP}(n,t) = \sqrt{\frac{P_T}{L}} \exp\left(\frac{j2\pi n(t-1)}{T_P}\right) \exp\left(\frac{j\pi(t-1)^2}{T_P}\right), \quad n = 1, 2, ..., L,\ t = 1, 2, ..., T_P. \quad (44)$$

Note that the length of $\mathbf{S}_{UP}$ might be different from that of $\mathbf{S}_{DP}$, which can be adjusted given the practical requirements. If Φ is perfectly estimated, the signal received at the BS is

$$\begin{aligned} \mathbf{Y}_{UL} &= \sum_{l=1}^{L} \beta_l \mathbf{a}(\theta_l) \mathbf{b}^T(\phi_l) \mathbf{F}_{UE} \tilde{\mathbf{S}}_{UP,l} + \mathbf{N}_{UL} \\ &= \sum_{l=1}^{L} \beta_l \mathbf{a}(\theta_l) \tilde{\mathbf{S}}_{UP,l} + \mathbf{N}_{UL}, \end{aligned} \quad (45)$$

where $\tilde{\mathbf{S}}_{UP,l}$ is defined as the reference UP signal in the (p_l, q_l)th range-Doppler bin. To identify Θ_1, the BS formulates the new analog combiner $\mathbf{G}_{RF} \in \mathbb{C}^{K \times N_{BS}}$ with *K* RF chains being activated, where the *k*th row of $\mathbf{G}_{RF}$ is given as

$$\mathbf{G}_{RF}(k,:) = \mathbf{a}^H\left(\hat{\theta}_k\right), \forall k. \quad (46)$$

After analog combination, the BS picks the specific L entries having the L largest moduli from $\mathbf{G}_{RF}\mathbf{Y}_{UL}\mathbf{1}_{T+P}$. This is equivalent to identifying the L RF chains that output the L largest signal power, generated by the signals arriving from *L* AoAs $\theta_l, \forall l$ of the communication channel. By doing so, the BS can identify Θ_1 from Θ.

The next step is to estimate the remaining parameters for each communication path, such that they could be compensated at the stage of downlink communication. Following a similar procedure of Sec. V-B, we estimate the delay and Doppler parameters by the MF Algorithm, and the scattering coefficients $\beta_l, \forall l$ by the APES method. For clarity, we summarize the target search/channel estimation process in Algorithm 2.

Algorithm 2 Stage 1: Radar Target Search and Communication Channel Estimation

Step 1: BS sends DP to search targets and estimate the channel.
Step 2: BS receives the echo wave from targets, and estimates θ_k, p_k, q_k and α_k using MUSIC, MF and APES algorithms for each target, respectively.
Step 3: UE receives DP, and estimates ϕ_l for each communication path using MUSIC.
Step 4: UE formulates the ZF beamformer based on (43), and transmits UP.
Step 5: BS receives the UP, identifies the communication paths by the analog combiner (46), and estimates $\tilde{p}_l$, $\tilde{q}_l$ and β_l using the MF and APES for each communication path, respectively.

VI. Stage 2: Radar Transmit Beamforming and Downlink Communication

In this section, we propose a novel joint transmit beamforming design at the BS for both target detection and DL communication by invoking the HAD structure. For supporting the radar functionality, we formulate directional beams towards the targets of interest to obtain more accurate observations. For the communication aspect, on the other hand, we equalize the channel.

Remark 7: Due to the Doppler shift and the time delay for each communication path, the received signal at the UE will be distorted. Fortunately, given the estimated delay and Doppler shift parameters above, it is possible for the BS to precompensate these effects individually at each RF chain/beam via exploiting the high angular resolution of the mMIMO array. In this case, existing compensation methods such as [133]–[136] could be readily applied. To avoid deviation of the core of our paper and for ease of discussion, we will focus on the spatial processing only in the remainder of the paper, and assume that both the Doppler and delay effects in the channel are perfectly compensated.

A. Problem Formulation

Our goal is to design the analog and the digital beamforming matrices $\mathbf{F}_{RF}$ and $\mathbf{F}_{BB}$ to jointly approach the ideal radar and communication beamformers. Recalling that $L \leq N_{UE} \leq N_{BS}$, the communication channel has a rank of L, which supports a maximum of L independent data streams to be transmitted simultaneously. Nevertheless, we use a digital beamformer with larger size $\mathbf{F}_{BB} \in \mathbb{C}^{K \times K}$ since we have to formulate extra beams towards the radar targets. In addition, the proposed method requires $\mathbf{F}_{BB}$ to have a full rank of K. Accordingly, *K* RF chains are activated, leading to an $N_{BS} \times K$ analog beamformer. The signal vector received at the UE can therefore be expressed as

$$\begin{aligned} \mathbf{y}_{DL} &= \mathbf{B}(\Phi) \operatorname{diag}(\boldsymbol{\beta}) \mathbf{A}^T(\Theta_1) \mathbf{F}_{RF} \mathbf{F}_{BB} \mathbf{s} + \mathbf{n}_{DL} \\ &\triangleq \mathbf{H} \mathbf{F}_{RF} \mathbf{F}_{BB} \mathbf{s} + \mathbf{n}_{DL}, \end{aligned} \quad (47)$$

where $\mathbf{H} = \mathbf{B}(\Phi) \operatorname{diag}(\boldsymbol{\beta}) \mathbf{A}^T(\Theta_1)$ is the rank-*L* communication channel matrix, $\mathbf{n}_{DL}$ denotes the noise vector with variance σ_{DL}^2, $\mathbf{s} \in \mathbb{C}^{K \times 1}$ denotes the transmit signal vector, which can be further decomposed as

$$\mathbf{s} = \begin{bmatrix} \mathbf{s}_1 \\ \mathbf{s}_2 \end{bmatrix}, \quad (48)$$

where $\mathbf{s}_1 \in \mathbb{C}^{L\times 1}$ and $\mathbf{s}_2 \in \mathbb{C}^{(K-L)\times 1}$ are statistically independent of each other. Each entry of $\mathbf{s}$ is assumed to follow a standard Gaussian distribution. Note that while both $\mathbf{s}_1$ and $\mathbf{s}_2$ are exploited for radar target detection, only $\mathbf{s}_1$ is exploited for DL communication whereas $\mathbf{s}_2$ contains no useful information, as the communication channel only supports transmission of L independent data streams .

Note that a pseudo inverse is unobtainable for the channel $\mathbf{H}$ since neither $\mathbf{H}\mathbf{H}^H$ nor $\mathbf{H}^H\mathbf{H}$ is invertible. Therefore, both transmit and receive beamformings are required for equalizing the channel. By introducing $\tilde{\mathbf{H}} \triangleq \mathrm{diag}\left(\boldsymbol{\beta}\right)\mathbf{A}^T\left(\Theta_1\right)$, the channel $\mathbf{H}$ can be equivalently expressed as $\mathbf{H} = \mathbf{B}\left(\Phi\right)\tilde{\mathbf{H}}$. Noting that both $\tilde{\mathbf{H}}$ and $\mathbf{B}\left(\Phi\right)$ have a full rank of L, and that they have been estimated at the BS and the UE respectively, we can formulate the corresponding zero-forcing (ZF) beamformers as

$$\begin{aligned}\mathbf{F}_{BS} &= \tilde{\mathbf{H}}^H\left(\tilde{\mathbf{H}}\tilde{\mathbf{H}}^H\right)^{-1},\\ \mathbf{W}_{UE} &= \left(\mathbf{B}^H\left(\Phi\right)\mathbf{B}\left(\Phi\right)\right)^{-1}\mathbf{B}^H\left(\Phi\right).\end{aligned} \tag{49}$$

While $\mathbf{W}_{UE}$ can be implemented as a fully-digital beamformer at the UE, $\mathbf{F}_{BS}$ can only be approximately approached by the hybrid array at the BS. In the meantime, the beamformer $\mathbf{F}_D = \mathbf{F}_{RF}\mathbf{F}_{BB}$ designed should also steer the beams towards all the *K* targets. Note that this is equivalent to designing the covariance matrix of the transmit signal, which is formulated as

$$\begin{aligned}\mathbf{R}_s &= \mathbb{E}\left(\mathbf{F}_D\mathbf{s}\mathbf{s}^H\mathbf{F}_D^H\right) = \mathbf{F}_D\mathbb{E}\left(\mathbf{s}\mathbf{s}^H\right)\mathbf{F}_D^H\\ &= \mathbf{F}_{RF}\mathbf{F}_{BB}\mathbf{F}_{BB}^H\mathbf{F}_{RF}^H.\end{aligned} \tag{50}$$

In what follows, we propose a low-complexity approach to the design of both $\mathbf{F}_{RF}$ and $\mathbf{F}_{BB}$.

B. Low-complexity Approach for DFRC Hybrid Beamforming Design

Based on the discussions above, a straightforward approach is to formulate each column of $\mathbf{F}_{RF}$ based on the steering vector associated with all the K angles, yielding

$$\mathbf{F}_{RF}\left(:,k\right) = \mathbf{a}^*\left(\theta_k\right), \forall k = 1,2,\cdots,K. \tag{51}$$

Nevertheless, the above $\mathbf{F}_{RF}$ does not guarantee having a desired transmit beampattern, which also depends on $\mathbf{F}_{BB}$. From (13) and (50), it becomes plausible that the transmit beampattern is solely dependent on $\mathbf{F}_{RF}$ if $\mathbf{F}_{BB}$ is an unitary matrix. In this case, the overall beamforming design is capable of guaranteeing the formulation of *K* narrow beams towards radar targets. To show this, we fix $\mathbf{F}_{RF}$ as (51) while assuming $\mathbf{F}_{BB}\mathbf{F}_{BB}^H = \frac{P_T}{KN_{BS}}\mathbf{I}_K$. The transmit beampattern can be accordingly given as

$$\begin{aligned}d\left(\theta\right) &= \mathbf{a}^T\left(\theta\right)\mathbf{R}_s\mathbf{a}^*\left(\theta\right) = \frac{P_T}{KN_{BS}}\mathbf{a}^T\left(\theta\right)\mathbf{F}_{RF}\mathbf{F}_{RF}^H\mathbf{a}^*\left(\theta\right)\\ &= \begin{cases}\dfrac{P_T}{KN_{BS}}\left(N_{BS}^2 + \sum\limits_{\substack{k=1\\k\neq i}}^{K}\left|\mathbf{a}^T\left(\theta\right)\mathbf{a}^*\left(\theta_k\right)\right|^2\right), \theta = \theta_i \in \Theta, \forall i,\\ \dfrac{P_T}{KN_{BS}}\sum\limits_{k=1}^{K}\left|\mathbf{a}^T\left(\theta\right)\mathbf{a}^*\left(\theta_k\right)\right|^2, \theta \notin \Theta.\end{cases}\end{aligned} \tag{52}$$

When N_{BS} is sufficient large, $\left|\mathbf{a}^T\left(\theta_i\right)\mathbf{a}^*\left(\theta_k\right)\right|^2$ will be much smaller than N_{BS}^2 for any $i \neq k$, and thus a peak only appears if $\theta \in \Theta$.

In order to guarantee both the radar and the communication's performance under the unitary constraint imposed on $\mathbf{F}_{BB}$, we consider the following optimization problem by fixing $\mathbf{F}_{RF}$ as (51), yielding

$$\begin{aligned}\min_{\mathbf{F}_{BB}}\ &\left\|\mathbf{F}_{RF}\mathbf{F}_{BB} - \left[\mathbf{F}_{BS}, \mathbf{F}_{aux}\right]\right\|_F^2\\ s.t.\ \ &\mathbf{F}_{BB}\mathbf{F}_{BB}^H = \frac{P_T}{KN_{BS}}\mathbf{I}_K,\end{aligned} \tag{53}$$

where $\mathbf{F}_{BS} \in \mathbb{C}^{N_{BS}\times L}$ is defined in (49), and $\mathbf{F}_{aux} \in \mathbb{C}^{N_{BS}\times(K-L)}$ is an auxiliary matrix that is to be designed later. The scaling factor $\frac{P_T}{KN_{BS}}$ ensures satisfying the total transmit power budget of $\left\|\mathbf{F}_{RF}\mathbf{F}_{BB}\right\|_F^2 = P_T$. To be specific, the problem (53) aims for approximating the fully-digital ZF beamformer $\mathbf{F}_{BS}$ by the first L columns of $\mathbf{F}_D$. The orthogonality constraint on $\mathbf{F}_{BB}$ ensures that the transmit beampattern remians unchanged, given the analog beamformer defined in (51). While problem (53) is non-convex, it can be efficiently solved in closed-form by using the following proposition.

Proposition 1. *The globally optimal solution of (53) can be obtained in closed-form as*

$$\mathbf{F}_{BB} = \sqrt{\frac{P_T}{KN_{BS}}}\tilde{\mathbf{U}}\tilde{\mathbf{V}}^H, \tag{54}$$

where

$$\tilde{\mathbf{U}}\tilde{\mathbf{\Sigma}}\tilde{\mathbf{V}}^H = \mathbf{F}_{RF}^H\left[\mathbf{F}_{BS}, \mathbf{F}_{aux}\right] \tag{55}$$

is the singular value decomposition (SVD) of $\mathbf{F}_{RF}^H\left[\mathbf{F}_{BS}, \mathbf{F}_{aux}\right]$.

Proof. See Appendix A. ■

C. Spectral Efficiency Evaluation

We then evaluate the performance of the communication by computing the spectral efficiency (SE). Let us firstly split the designed beamforming matrix as

$$\mathbf{F}_D = \mathbf{F}_{RF}\mathbf{F}_{BB} = \mathbf{F}_{RF}\left[\mathbf{F}_{BB,1}, \mathbf{F}_{BB,2}\right], \tag{56}$$

where $\mathbf{F}_{BB,1} \in \mathbb{C}^{K\times L}, \mathbf{F}_{BB,2} \in \mathbb{C}^{K\times(K-L)}$. By recalling (48), and multiplying (47) with $\mathbf{W}_{UE}$, the post-processing signal vector at the UE can be formulated by

$$\begin{aligned}\tilde{\mathbf{y}}_{DL} &= \sqrt{\rho_{DL}}\mathbf{W}_{UE}\mathbf{H}\mathbf{F}_{RF}\mathbf{F}_{BB}\mathbf{s} + \mathbf{W}_{UE}\mathbf{n}\\ &= \underbrace{\sqrt{\rho_{DL}}\mathbf{W}_{UE}\mathbf{H}\mathbf{F}_{RF}\mathbf{F}_{BB,1}\mathbf{s}_1}_{\text{Useful Signal}} + \underbrace{\sqrt{\rho_{DL}}\mathbf{W}_{UE}\mathbf{H}\mathbf{F}_{RF}\mathbf{F}_{BB,2}\mathbf{s}_2}_{\text{Interference}}\\ &\quad + \mathbf{W}_{UE}\mathbf{n}_{DL}.\end{aligned} \tag{57}$$

where ρ_{DL} stands for the average received power at the UE. The second term of (57) is the interference imposed on the UE as it contains no useful information. The spectral efficiency is therefore given as

$$R_{DL} = \log\det\left(\begin{matrix}\mathbf{I}_L + \dfrac{\rho_{DL}}{L}\mathbf{R}_{in}^{-1}\mathbf{W}_{UE}\mathbf{H}\mathbf{F}_{RF}\mathbf{F}_{BB,1}\\ \times\mathbf{F}_{BB,1}^H\mathbf{F}_{RF}^H\mathbf{H}^H\mathbf{W}_{UE}^H\end{matrix}\right), \tag{58}$$

where $\mathbf{R}_{in}$ is the covariance matrix of the interference plus noise, which is

$$\mathbf{R}_{in} = \rho_{DL}\mathbf{W}_{UE}\mathbf{H}\mathbf{F}_{RF}\mathbf{F}_{BB,2}\mathbf{F}_{BB,2}^H\mathbf{F}_{RF}^H\mathbf{H}^H\mathbf{W}_{UE}^H + \sigma_c^2\mathbf{W}_{UE}\mathbf{W}_{UE}^H. \quad (59)$$

D. Interference Reduction

The enhancement of SE requires addressing the interference term in (57). It can be observed that the interference power is mainly determined by $\mathbf{F}_{RF}\mathbf{F}_{BB,2}$, which is designed to approach $\mathbf{F}_{aux}$ in the optimization problem (53). Hence, the choice of $\mathbf{F}_{aux}$ is key to the hybrid beamforming design.

HBF-Null Design: As an intuitive method, one may choose $\mathbf{F}_{aux}$ as a null-space projection (NSP) matrix, such that $\tilde{\mathbf{H}}\mathbf{F}_{aux} = \mathbf{0}$. This can be realized by firstly performing the SVD of $\tilde{\mathbf{H}}$, and then choosing the right singular vectors associated with zero singular values as the columns of $\mathbf{F}_{aux}$. By doing so, the solution of (53) will satisfy that $\tilde{\mathbf{H}}\mathbf{F}_{RF}\mathbf{F}_{BB,2} \approx \mathbf{0}$ and thus $\mathbf{H}\mathbf{F}_{RF}\mathbf{F}_{BB,2} \approx \mathbf{0}$.

HBF-Opt Design: To further mitigate the interference, we consider another option by letting $\mathbf{F}_{aux} = \mathbf{0}$. While it is impossible to approach zero by multiplying the right side of $\mathbf{F}_{RF}$ with any unitary matrix, we show that such a method brings significant benefits by proving the following proposition.

Proposition 2. *The interference can be completely eliminated by solving (53) upon letting* $\mathbf{F}_{aux} = \mathbf{0}$.

Proof. See Appendix B. ■

The intuition behind the HBF-Opt method is simple. Based on (54) and (56), $\mathbf{F}_{BB,1}$ is obtained by letting all the non-zero singular values of $\mathbf{F}_{RF}^H\mathbf{F}_{BS}$ be 1. As a result, $\mathbf{F}_{RF}\mathbf{F}_{BB,1}$ is an approximation of $\mathbf{F}_{BS}$. By letting $\mathbf{F}_{aux} = \mathbf{0}$, $\mathbf{F}_{BB,2}$ belongs to the null-space of $\mathbf{F}_{RF}^H\mathbf{F}_{BS}$, and thus belongs to the null-space of $\mathbf{H}\mathbf{F}_{RF}$ given the pseudo-inverse structure of $\mathbf{F}_{BS}$. Therefore, the interference of $\mathbf{s}_2$ is zero-forced.

VII. Stage 3: Radar Target Tracking and Uplink Communication

After the joint transmission of radar and communication signals, the BS receives both the echo wave from the targets and the communication data from the UE. In this section, we propose a novel approach for joint radar target tracking and UL communication by relying on the knowledge of the previously estimated channel and target parameters. Again, to avoid deflection of our focus, here we consider only the tracking of the AoAs and AoDs of the targets, and assume that the Doppler and delay effects are well-compensated.

A. Receive Signal Model

According to the frame structure designed in Fig. 3, the signal received at the BS may fall into 2 categories: 1) Non-overlapped radar echo and UL communication signal and 2) overlapped signals. Since in the non-overlapped case both signals are interference-free, they can be readily processed using the conventional approaches. We therefore focus our attention on the overlapped case, where the radar and communication signals are partially interfering with each other.

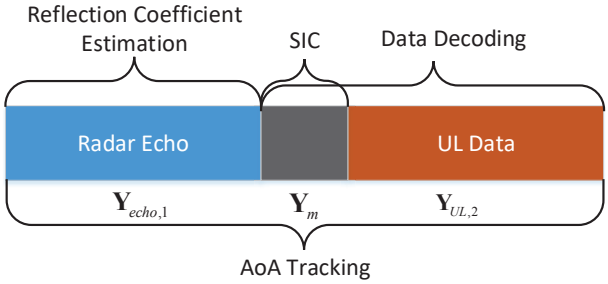

Fig. 5. Overlapped receive signal model.

We show a generic model of the overlapped case in Fig. 5, where the overlapped period is marked as black. The received signal can be expressed as

$$\mathbf{Y}_0 = [\mathbf{Y}_{echo,1}, \mathbf{Y}_m, \mathbf{Y}_{UL,2}] \in \mathbb{C}^{N_{BS}\times T_0}, \quad (60)$$

where $\mathbf{Y}_{echo,1} \in \mathbb{C}^{N_{BS}\times(T_{DL}-\Delta T)}$ denotes the non-interfered part of the radar echo wave, $\mathbf{Y}_m \in \mathbb{C}^{N_{BS}\times\Delta T}$ represents the mixture of the echo wave and the communication signal received from the UE with ΔT being the length of the overlapping period, and finally $\mathbf{Y}_{UL,2} \in \mathbb{C}^{N_{BS}\times(T_{UL}-\Delta T)}$ stands for the non-interfered part of the UE signal with T_{UL} being the length of the UL frame. It can be readily seen that $T_0 = T_{DL} + T_{UL} - \Delta T$.

By using the same notations from the previous sections, the above three signal matrices can be expressed as

$$\mathbf{Y}_{echo,1} = \mathbf{A}\left(\hat{\Theta} + \Delta\Theta\right)\mathrm{diag}\left(\tilde{\boldsymbol{\alpha}}\right)\mathbf{A}^T\left(\hat{\Theta} + \Delta\Theta\right)\mathbf{X}_{r,1} + \mathbf{Z}_1, \quad (61)$$

$$\begin{aligned}\mathbf{Y}_m &= \mathbf{Y}_{echo,2} + \mathbf{Y}_{UL,1} \\ &= \mathbf{A}\left(\hat{\Theta} + \Delta\Theta\right)\mathrm{diag}\left(\tilde{\boldsymbol{\alpha}}\right)\mathbf{A}^T\left(\hat{\Theta} + \Delta\Theta\right)\mathbf{X}_{r,2} \\ &+\mathbf{A}\left(\hat{\Theta}_1 + \Delta\Theta_1\right)\mathrm{diag}\left(\tilde{\boldsymbol{\beta}}\right)\mathbf{B}^T\left(\hat{\Phi} + \Delta\Phi\right)\mathbf{X}_{UL,1} + \mathbf{Z}_m,\end{aligned} \quad (62)$$

$$\mathbf{Y}_{UL,2} = \mathbf{A}\left(\hat{\Theta}_1 + \Delta\Theta_1\right)\mathrm{diag}\left(\tilde{\boldsymbol{\beta}}\right)\mathbf{B}^T\left(\hat{\Phi} + \Delta\Phi\right)\mathbf{X}_{UL,2} + \mathbf{Z}_2, \quad (63)$$

where $\hat{\Theta}$, $\hat{\Theta}_1 \subseteq \hat{\Theta}$ and $\hat{\Phi}$ contain the AoAs of all the K targets, the AoAs and the AoDs of the UL channel (which are the AoDs and the AoAs of the DL channel, respectively) estimated in the last PRI, $\Delta\Theta$, $\Delta\Theta_1$ and $\Delta\Phi$ represent accordingly the variations plus the estimation errors in these angles in the current PRI. Furthermore, $\tilde{\boldsymbol{\alpha}}$ contains the complex reflection coefficients of all the K targets, while $\tilde{\boldsymbol{\beta}}$ contains the complex scattering coefficients of L communication paths. Referring to (61) and (63), $\mathbf{X}_{r,1}$ and $\mathbf{X}_{UL,2}$ are the non-interfered parts of the radar and communication signals, while $\mathbf{X}_{r,2}$ and $\mathbf{X}_{UL,1}$ are the signals in the overlapped period, and finally $\mathbf{Z}_1, \mathbf{Z}_m, \mathbf{Z}_2$ denote the Gaussian noise matrices.

To track the targets, the current AoAs and AoDs have to be estimated based on the previously estimated angles. As the angles are slowly varying as compared to the movement of the

targets, we assume that these variations are relatively small. In contrast to the AoAs and AoDs, we assume that both $\tilde{\boldsymbol{\alpha}}$ and $\tilde{\boldsymbol{\beta}}$ are random realizations that are independent of those of the last PRI, and hence have to be estimated again. Furthermore, we denote the transmitted signal in the PRI as

$$\mathbf{X}_r = [\mathbf{X}_{r,1}, \mathbf{X}_{r,2}] \in \mathbb{C}^{N_{BS} \times T_{DL}}, \tag{64}$$

which has been precoded by $\mathbf{F}_{RF}$ and $\mathbf{F}_{BB}$ designed in Stage 2, where $\mathbf{F}_{RF}$ generates *K* beams towards the estimated AoAs in $\hat{\Theta}$. Finally, the UL communication signal is given by

$$\mathbf{X}_{UL} = [\mathbf{X}_{UL,1}, \mathbf{X}_{UL,2}] \in \mathbb{C}^{N_{UE} \times T_{UL}}, \tag{65}$$

which has been precoded at the UE by $\mathbf{F}_{UE}$ in (43) with the knowledge of the previously estimated $\hat{\Phi}$. Note that both $\mathbf{X}_r$ and $\mathbf{X}_{UL}$ are assumed to be Gaussian distributed following the previous assumptions. For the sake of convenience, we employ the assumption that the BS can reliably identify the beginning of $\mathbf{X}_{UL}$. This can be realized by inserting synchronization sequences at the beginning of the $\mathbf{X}_{UL}$. The designed sequences should be orthogonal to the radar signal $\mathbf{X}_r$, such that the interference of the echo wave can be mitigated at the synchronization stage[6].

In what follows, we propose approaches for both target tracking and UL signal processing.

B. Target Tracking

After receiving $\mathbf{Y}_0$, the first step is analog combination, which gives us

$$\begin{aligned} &\tilde{\mathbf{Y}}_0 = \mathbf{W}_{RF}\mathbf{Y}_0 \\ &= [\mathbf{W}_{RF}\mathbf{Y}_{echo,1}, \mathbf{W}_{RF}\mathbf{Y}_m, \mathbf{W}_{RF}\mathbf{Y}_{UL,2}] \in \mathbb{C}^{N_{RF} \times T_0}, \end{aligned} \tag{66}$$

where we activate all N_{RF} RF chains to formulate an analog combination matrix $\mathbf{W}_{RF} \in \mathbb{C}^{N_{RF} \times N_{BS}}$. To exploit the knowledge of the estimated angles in $\hat{\Theta}$, the first *K* rows of $\mathbf{W}_{RF}$ (which represent the phase shifters linked with the first *K* RF chains) are set as

$$\mathbf{W}_{RF}(k,:) = \mathbf{a}^H\left(\hat{\theta}_k\right), \forall k, \tag{67}$$

which indicates that the receive beams are pointing to the previously estimated AoAs. The phase shifters in the remaining RF chains are randomly set, thus for creating redundant observations of the received data in order to improve the estimation accuracy.

An important fact that can be observed from (61)-(63) is that the mutual interference signal in (62) will not degrade the AoA estimation performance. Instead, it may provide benefits in estimating some of the AoAs. This is because the BS receives both the echo waves and the communication signals from the angles in $\Theta_1 + \Delta\Theta_1$. As a result, the signal associated with these angles may have higher power than that associated with others, hence leading to better estimation performance.

[6]Note that such synchronization sequences can be easily formulated as the null-space projection matrix of the radar signal. Nevertheless, the data sequences that contain information from the UE are unlikely to be orthogonal to the radar signal. Hence, we still need to mitigate the radar interference when processing the communication signal after synchronization.

Given the small variations in the AoAs, one may search in the small intervals within each $\hat{\theta}_k, \forall k$ instead of searching the whole angular domain. We therefore propose to apply the MUSIC algorithm to $\tilde{\mathbf{Y}}_0$ for estimating the AoAs. For each $\hat{\theta}_k$, we search for peaks in the MUSIC spectrum (31) within $\left[\hat{\theta}_k - \Delta_{\max}, \hat{\theta}_k + \Delta_{\max}\right]$, where $\Delta_{\max}$ is the maximum angular variation of the targets.

C. Uplink Communication

In this subsection, we propose a promising technique for estimating the remaining target parameters and decode the communication signals. Since $\mathbf{Y}_{echo,1}$ is not interfered by the communication signal, it can be used to estimate the target reflection coefficients $\tilde{\boldsymbol{\alpha}}$. With the estimated AoAs at hand, one can apply the APES approach to obtain an estimate of $\tilde{\alpha}_k$, i.e., $\hat{\tilde{\alpha}}_k$ for each angle.

The communication signal can then be recovered by the SIC approach. Given the estimated parameters and $\mathbf{X}_r$, the target reflections can be reconstructed as

$$\hat{\mathbf{Y}}_{echo} = \mathbf{A}\left(\hat{\Theta} + \Delta\hat{\Theta}\right) \mathrm{diag}\left(\hat{\tilde{\boldsymbol{\alpha}}}\right) \mathbf{A}^T\left(\hat{\Theta} + \Delta\hat{\Theta}\right) \mathbf{X}_r, \tag{68}$$

where $\Delta\hat{\Theta}$ denotes the estimated variations of AoAs. Note that by multiplying $\mathbf{W}_{RF}$, the $N_{BS} \times T_0$ matrix $\mathbf{Y}_0$ has been mapped to a lower-dimensional space having the size of $N_{RF} \times T_0$. Therefore, one can only recover the communication signal after low-complexity analog combination. By subtracting the radar signal estimated, the interfered communication signal in $\mathbf{Y}_m$ can be estimated as

$$\begin{aligned} &\mathbf{W}_{RF}\hat{\mathbf{Y}}_{UL,1} = \mathbf{W}_{RF}\mathbf{Y}_m \\ &-\mathbf{W}_{RF}\mathbf{A}\left(\hat{\Theta} + \Delta\hat{\Theta}\right) \mathrm{diag}\left(\hat{\tilde{\boldsymbol{\alpha}}}\right) \mathbf{A}^T\left(\hat{\Theta} + \Delta\hat{\Theta}\right) \mathbf{X}_{r,2}. \end{aligned} \tag{69}$$

Based on the above, the whole UL signal after analog combination can be expressed as

$$\mathbf{W}_{RF}\hat{\mathbf{Y}}_{UL} = \left[\mathbf{W}_{RF}\hat{\mathbf{Y}}_{UL,1}, \mathbf{W}_{RF}\mathbf{Y}_{UL,2}\right]. \tag{70}$$

Since the UL signal has been precoded by (43) at the UE, the steering matrix $\mathbf{B}^T\left(\hat{\Phi} + \Delta\Phi\right)$ has been eliminated with limited errors. The BS can simply obtain the estimates of the path-losses $\hat{\tilde{\boldsymbol{\beta}}}$ by the LS approach with the help of the known synchronization sequence, and construct a baseband ZF beamformer by computing the following pseudo-inverse

$$\mathbf{W}_{BB} = \left(\mathbf{W}_{RF}\mathbf{A}\left(\hat{\Theta}_1 + \Delta\hat{\Theta}_1\right) \mathrm{diag}\left(\hat{\tilde{\boldsymbol{\beta}}}\right)\right)^{\dagger}. \tag{71}$$

Upon multiplying $\mathbf{W}_{RF}\hat{\mathbf{Y}}_{UL}$ by $\mathbf{W}_{BB}$, the communication symbols can be finally decoded. For clarity, we summarize the signal processing procedures of Stage 3 in Algorithm 2.

D. Spectral Efficiency Evaluation

We round off this section by proposing a performance metric for the UL communication. While the estimated radar interference has been subtracted from $\mathbf{Y}_m$, there will still be some

Algorithm 3 Stage 3: Radar Target Tracking and UL Communication

Step 1: BS receives both target echoes and UL signals that are partially overlapped with each other.
Step 2: BS formulates an analog combiner $\mathbf{W}_{RF}$ based on estimated $\hat{\Theta}$ in the last PRI.
Step 3: BS estimates the reflection coefficients and the angular variation $\Delta\Theta$ by searching in a small interval within each $\hat{\theta}_k \in \hat{\Theta}$.
Step 4: BS recovers the radar echoes based on the estimates from Step 3, and removes the radar interference in the overlapped part of the received signal.
Step 5: BS formulates a ZF beamformer to equalize the communication channel, and decodes the UL data.

residual interference potentially degrading the communication performance. The residual interference can be expressed as

$$\begin{aligned}\mathbf{Y}_{res} = &\mathbf{A}\left(\hat{\Theta}+\Delta\Theta\right)\mathrm{diag}\left(\tilde{\boldsymbol{\alpha}}\right)\mathbf{A}^T\left(\hat{\Theta}+\Delta\Theta\right)\mathbf{X}_{r,2}\\ &-\mathbf{A}\left(\hat{\Theta}+\Delta\hat{\Theta}\right)\mathrm{diag}\left(\hat{\tilde{\boldsymbol{\alpha}}}\right)\mathbf{A}^T\left(\hat{\Theta}+\Delta\hat{\Theta}\right)\mathbf{X}_{r,2}\in\mathbb{C}^{N_{BS}\times\Delta T}.\end{aligned} \tag{72}$$

Fortunately, the above interference will only be active during the first ΔT symbols, in which case the spectral efficiency can be given by

$$R_1 = \log\det\begin{pmatrix}\mathbf{I}_L+\frac{\rho_{UL}}{L}\mathbf{R}_{in}^{-1}\mathbf{W}_{BB}\mathbf{W}_{RF}\mathbf{H}\mathbf{F}_{UE}\\ \times\mathbf{F}_{UE}^H\mathbf{H}^H\mathbf{W}_{RF}^H\mathbf{W}_{BB}^H\end{pmatrix}, \tag{73}$$

where

$$\mathbf{R}_{in} = \mathbf{W}_{BB}\mathbf{W}_{RF}\left(\frac{1}{\Delta T}\mathbf{Y}_{res}\mathbf{Y}_{res}^H+\sigma_{UL}^2\mathbf{I}_{N_{BS}}\right)\mathbf{W}_{RF}^H\mathbf{W}_{BB}^H \tag{74}$$

is the covariance matrix of the interference plus noise, and ρ_{UL} is the average received power at the BS. During the interference-free period having a length of $T_{UL}-\Delta T$, the spectral efficiency can be expressed as

$$R_2 = \log\det\begin{pmatrix}\mathbf{I}_L+\frac{\rho_{UL}}{L\sigma_{UL}^2}\left(\mathbf{W}_{RF}^H\mathbf{W}_{BB}^H\right)^{\dagger}\mathbf{H}\mathbf{F}_{UE}\\ \times\mathbf{F}_{UE}^H\mathbf{H}^H\mathbf{W}_{RF}^H\mathbf{W}_{BB}^H\end{pmatrix}. \tag{75}$$

The overall UL SE can be computed as the weighted summation of R_1 and R_2, which is

$$R_{UL} = \frac{\Delta T}{T_{UL}}R_1+\frac{T_{UL}-\Delta T}{T_{UL}}R_2. \tag{76}$$

VIII. Numerical Results

In this section, we provide numerical results to validate the performance of the proposed DFRC framework. Without loss of generality, the BS is assumed to be equipped with $N_{BS}=64$ antennas and $N_{RF}=16$ RF chains, which communicates with a UE having $N_{UE}=10$ antennas. Unless otherwise specified, we assume that the BS is detecting $K=8$ targets, wherein $L=4$ of them act as the scatterers in the communication channel. All the AoAs and AoDs are randomly drawn from the interval of $[-90^\circ, 90^\circ]$, which has been uniformly split into 180 slices. All the reflection and the scattering coefficients are assumed to obey the standard complex Gaussian distribution. The number of range and Doppler bins are set as $P=40, Q=30$. Finally, the maximum angular Doppler frequency is $\Omega=0.3\pi$ rad/s.

A. Radar Target Search and Channel Estimation

We first show the performance of Stage 1 in Fig. 6 with the aid of target search and channel estimation results. More specifically, in Fig. 6(a)-(c), we show the target estimation performance for a single channel realization at SNR $=10$dB for both DL and UP. We use a 64×140 LFM signal matrix as the DP, and a 4×140 LFM signal as the UP. We compare the estimated results to the true values for angle, range and Doppler parameters. It can be observed that by using the MUSIC, MF and APES methods, all the angles and the associated range-Doppler parameters can be accurately estimated. It is interesting to observe in Fig. 6(b) that two adjacent targets located at angles 31°,34°, range bins $8, 9$ can be clearly distinguished, which is because that they are resolvable at the Doppler axis as illustrated in Fig. 6(c).

We then consider another example in Fig. 6(d)-(f) at a low SNR $=-10$dB, where there are estimation errors in all the parameters. In Fig. 6(d), the BS fails to estimate the reflection coefficient of a weak target at -53° despite that it successfully estimates all the other 7 targets. Furthermore, the UE makes a wrong estimation at the angle of -69°. As the estimation of other parameters relies heavily on the initial angle estimation, there are estimation errors in range bins of both radar targets and communication scatterers. Nevertheless, it can be observed in Fig. 5(f) that most of these errors are small. Similar to Case 1, there are two targets in the adjacent range-Doppler bins as shown in Fig. 6(f). We see in Fig. 6(e) that our scheme is able to identify them given the fact that they are largely separated in the angular domain. These observations inspire us that even if two adjacent targets have the similar range-angle or range-Doppler parameters, one may distinguish them by exploiting the difference in the remaining parameter axis.

B. Radar Transmit Beamforming and Downlink Communication

Figs. 7-9 characterize the performance of Stage 2 in terms of the SE of the DL communication, the transmit beampattern and the number of the targets. In Fig. 7, we show the SE versus SNR of both perfect CSI and estimated CSI cases, where 'FD-ZF' denotes fully digital ZF beamforming, 'HBF-Opt' and 'HBF-Null' represent the hybrid beamforming designs proposed in Sec. VI-D with $\mathbf{F}_{aux}$ being zero and NSP matrices, respectively. There are slight SE performance-losses for the cases with estimated CSI, which suggests that the proposed channel estimation method guarantees a satisfactory communication performance. Furthermore, we see that in both the perfect and estimated CSI cases, the HBF-Opt design outperforms the HBF-Null design by approaching the performance of the fully digital ZF beamformer, which verifies our derivation on interference reduction.

Fig. 8 shows the transmit beampattern for both the

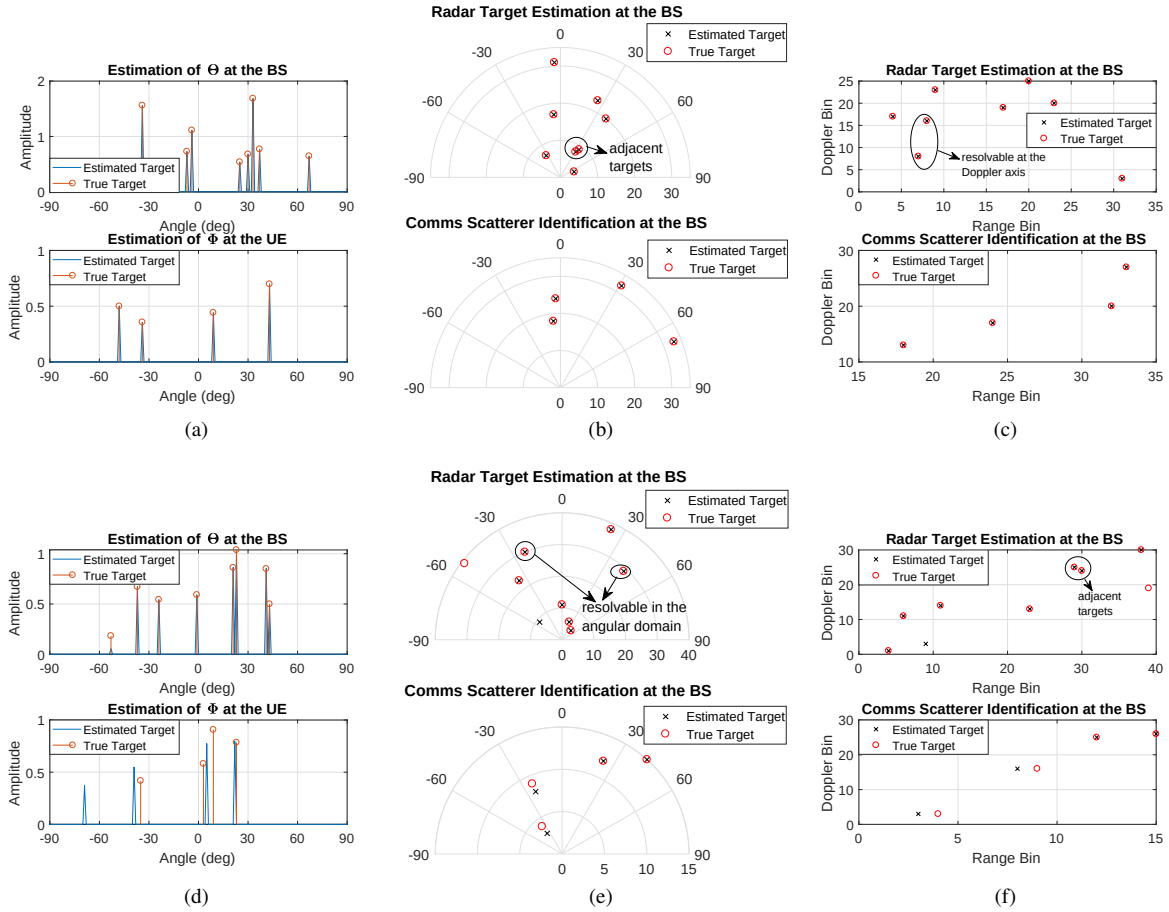

Fig. 6. Parameter estimation performance. (a) Angle estimation for Case 1, SNR $= 10$dB; (b) Angle and range estimation for Case 1, SNR $= 10$dB; (c) Range and Doppler estimation for Case 1, SNR $= 10$dB; (d) Angle estimation for Case 2, SNR $= -10$dB; (e) Angle and range estimation for Case 2, SNR $= -10$dB; (f) Range and Doppler estimation for Case 2, SNR $= -10$dB.

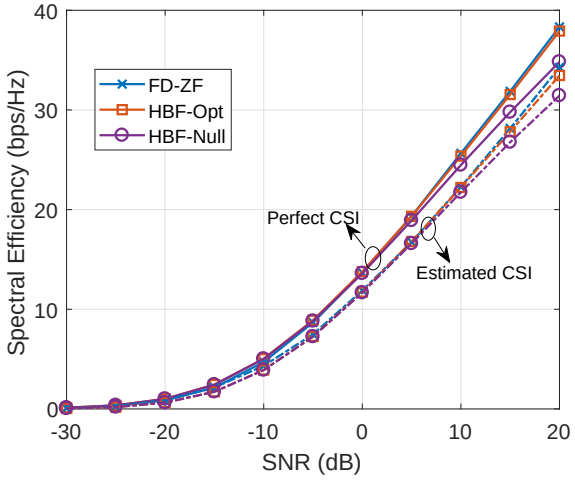

Fig. 7. Spectral efficiency of the DL communication by using (58).

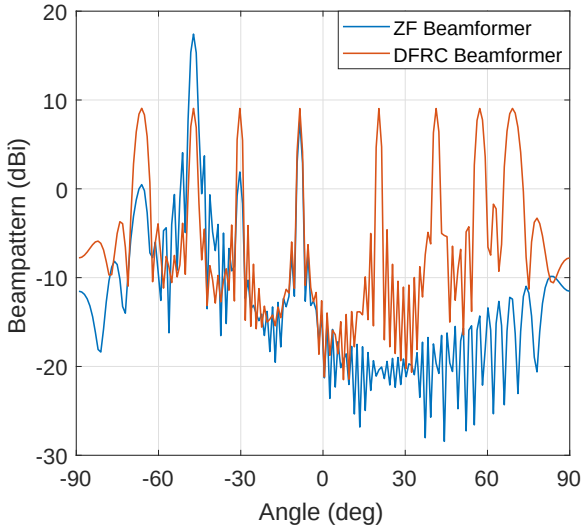

Fig. 8. Transmit beampatterns for the communication-only ZF beamformer and the proposed DFRC beamformers.

communication-only ZF beamformer and for the HBF beamformers designed for the DFRC system proposed. While the HBF-Opt and the HBF-Null designs employ different unitary matrices as $\mathbf{F}_{BB}$, the resultant beampatterns are the same since they use the same $\mathbf{F}_{RF}$. It can be seen that the

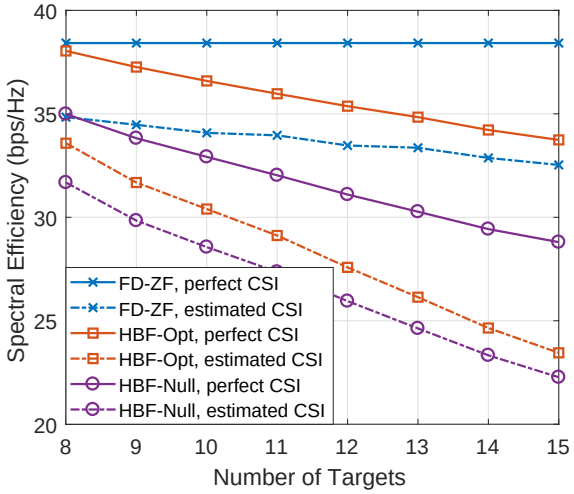

Fig. 9. Tradeoff between the spectral efficiency and the number of targets, SNR $=$ 20dB.

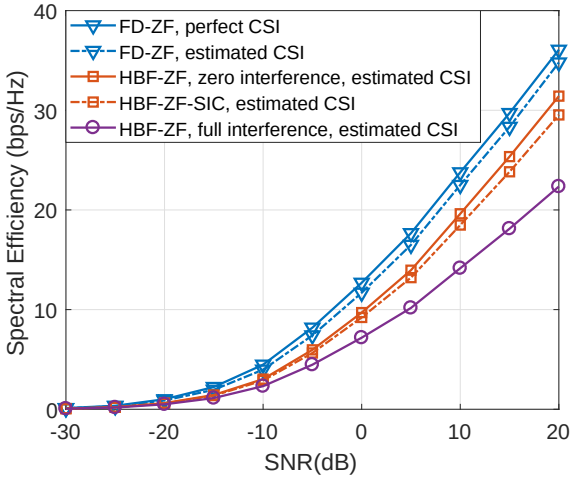

Fig. 10. Spectral efficiency of the UL communication by using (76), 30% overlapped ratio.

ZF beamformer only formulates beams towards 4 scatterers in the communication channel, and thus fails to track the extra 4 targets. By contrast, the proposed DFRC beamformer successfully generates 8 beams towards all the 8 targets.

To explicitly illustrate the performance tradeoff between radar and communication, we show in Fig. 9 the DL spectral efficiency by varying the number of targets at SNR $=$ 20dB, where we fix the number of scatterers in the communication channel as $L = 4$, and increase the total number of targets from $K = 8$ to 15. Since illuminating more targets requires more transmit power, less power is allocated to beams towards AoAs of the communication scatterers, leading to a reduced SINR. As a result, the DL SE decreases upon increasing the number of targets. Again, the SE of the HBF-Opt design is larger than that of the HBF-Null design. It is also interesting to observe the reduced SE of the fully digital ZF beamformer using estimated CSI, as the channel estimation becomes inaccurate owing to the newly added targets.

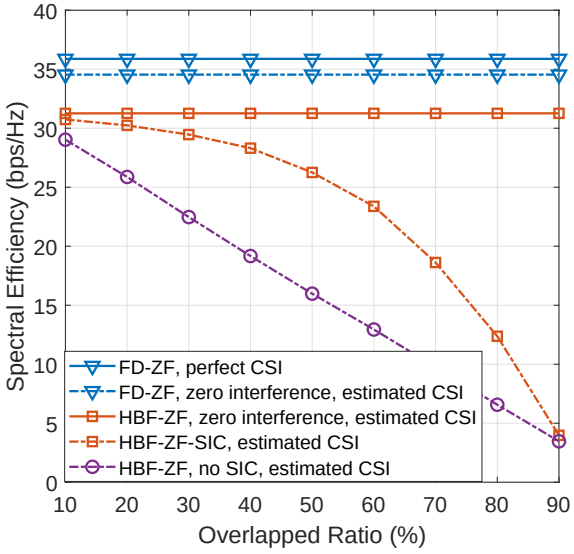

Fig. 11. Tradeoff between the spectral efficiency and the overlapped ratio, SNR $=$ 20dB.

C. Radar Target Tracking and Uplink Communication

Finally, we provide results for Stage 3 in Figs. 10-13, where we assume that the angle parameters of all the 8 targets of the previous PRI are perfectly known, based on which the DFRC system tracks the variation of the angles in the current PRI, while performing UL communications. As the angle parameters typically vary slowly in realistic scenarios, we assume without loss of generality that the variation of each angle is less than $\Delta_{\max} = 1^\circ$ at each PRI, which is reasonable for a PRI of a few of milliseconds. The DL and UL frame lengths are set to 140. The communication signal and the target echo wave are overlapped with each other, and share the same SNR. While it is known that the equivalent SNR scenario is the worst case for the SIC-based approaches, we will show next that our method can still achieve good performance. For notational convenience, "FD-ZF" represents the receive beamforming using a fully digital ZF beamformer at the BS, while "HBF-ZF" stands for the hybrid receive beamforming design proposed in Sec. VII, where the analog and the digital beamformers are given by (67) and (71), respectively.

Fig. 10 shows the UL SE performance of the proposed approach in Sec. VII. It is noteworthy that by using the SIC method proposed, the SE of the communication significantly increases compared to the cases with full radar echo interference in the overlapped period. Fig. 11 further illustrates the UL SE performance given the increased overlapped period ΔT, where the overlapping ratio is defined as $\Delta T/T$. We see that the SE becomes worse for longer overlapped period, in which case the interference of the radar echo is not cancelled thoroughly, and the residual interference power may have a grave impact on the UL communication performance. When the overlapped period is short, the performance gain obtained by the SIC approach is marginal since the interference from the radar echo is small enough. On the other hand, when the

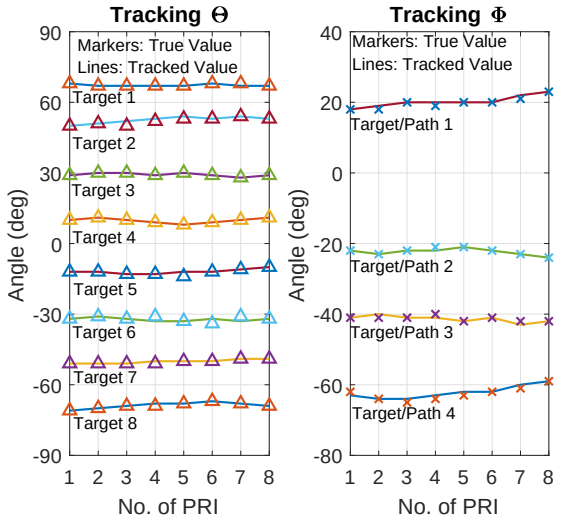

Fig. 12. Angle tracking performance at the BS and the UE, SNR $= -20$dB.

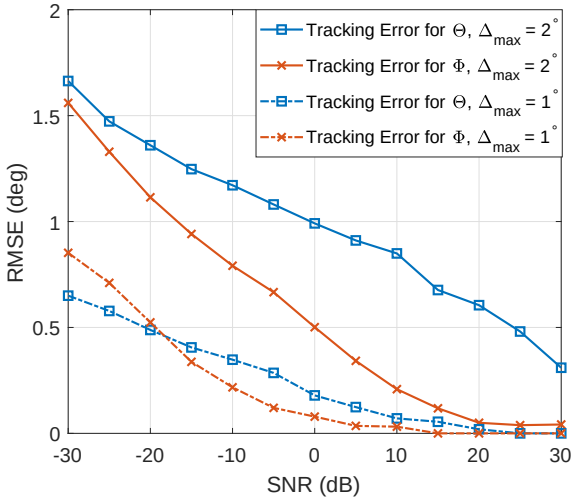

Fig. 13. Angle tracking RMSE vs. SNR.

overlapped ratio is greater than 90%, the BS fails to recover the radar signal, and thus is unable to cancel the interference by using the SIC, which also leads to modest performance gain. Nevertheless, in most overlapping cases, the SIC approach works well by considerably improving the SE.

In Fig. 12, we evaluate the performance of the proposed target tracking approach, where we compare the tracking results and the true variation for the AoAs Θ of the targets and the AoDs Φ of the scattering paths at SNR $= -20$dB for both target echoes and the communication signals. Note that the angles in Θ are estimated at the BS using both the target echoes and the UL signals, while the angles in Φ are estimated at the UE. It can be seen that all the angles can be accurately tracked with slight tracking errors despite the low SNR, which verifies again the effectiveness of the proposed method. Similar results are observed in Fig. 13, where we show the root-mean-squared-error (RMSE) of the proposed target tracking approach versus the SNR. It is shown that the RMSE for all the estimations is less than 1° at most of the SNR values for both $\Delta_{\max} = 1^\circ$ and 2°.

IX. Conclusion and Future Research

A. Summary of the Proposed Approaches

In this paper, we have reviewed the application scenarios and recent research progress in the area of communication and radar spectrum sharing (CRSS). We have proposed a novel dual-functional radar-communication (DFRC) system architecture that operates in the mmWave band, and is equipped with a massive MIMO antenna array and a hybrid analog-digital beamforming structure. We have further designed a novel TDD frame structure that can unify the radar and communication operations into 3 stages, namely 1) radar target search and channel estimation, 2) radar transmit beamforming and DL communication and 3) radar target tracking and UL communication. Accordingly, we have proposed joint signal processing strategies for each stage. In Stage 1, we aim for estimating the communication channel and searching for potential targets using orthogonal LFM signals generated by the HAD structure, while identifying the communication paths from the radar targets. In Stage 2, we have designed both analog and digital precoders for generating directional beams towards all the targets and scatterers, while pre-equalizing the impact of the communication channel. Finally in Stage 3, we have proposed a joint scheme for tracking the angular variation of all the targets, while decoding the UL communication signals by using the SIC approach. Simulation results have been provided to validate the proposed approaches, showing the feasibility of realizing both radar and communication functionalities on a single mmWave BS.

B. Future Works

While a number of contributions have been made towards radar-communication coexistence and joint radar-communication systems, the topic remains to be further explored within a broader range of constraints and scenarios. To this end, we list in the following a number of future research directions in the area.

1) Learning-based CRSS

A key challenge for CRSS is to distinguish between the echoes from targets and communication signals from users in the presence of noise and interference. In addition to the proposed joint receiver design for the mmWave system considered, it is also viable to apply machine learning (ML) based approaches, such as the independent component analysis (ICA) algorithm, for signal classification in more generic scenarios, given the independent statistical characteristics of the two kinds of signals. A recent example can be found in [75] where the compressed sensing (CS) approach is employed for joint parameter estimation and symbol demodulation. It is expected that by using advanced ML based techniques, the receiver design for CRSS can be well-addressed.

2) Security issues

Recent CRSS research has raised security and privacy concerns. By sharing the spectrum with communication systems,

the military radar may unintentionally give away vital information to commercial users, or even worse, to the adversary eavesdroppers. To this end, physical layer security must be considered in the CRSS scenarios, where a possible method is that radar actively transmits artificial noise (AN) to the adversary target to contaminate the eavesdropping, while formulating desired beampatterns. In the meantime, the communication performance also has to be guaranteed. Accordingly, a number of performance trade-offs involving the radar detection and estimation performance, the communication rate and the secrecy rate remain to be studied. Some initial works on this topic can be found in [137]–[139].

3) DFRC for V2X

As an important application scenario of the DFRC system, vehicular networks have recently drawn much attention from both industry and academia, where joint sensing and communications at the mmWave band is required. While the proposed approaches in this paper focus on mmWave cellular systems, it can be extended to V2X applications with the consideration of specific channel models for vehicle-to-vehicle (V2V) and vehicle-to-infrastructure (V2I) scenarios. Again, such schemes call for the design of novel beamforming/signaling approaches [112], [140].

4) Information theory aspects

To gain more in-depth insights into DFRC systems, information theoretical analysis is indispensable for revealing the fundamental performance limit. While existing contributions have considered the DFRC UL [77] as well as coexisting radar and communication systems [141], the DL DFRC channel needs further investigations. Here the key point is to view the radar targets as virtual energy receivers, and hence the DFRC transmission can be seen as the allocation of information and energy resources in the NLoS and LoS channels. From a higher-level perspective, one can also view the radar target as a relay, which receives the probing waveform and forwards it back to the radar, with its own parameter information being embedded in the echo wave. As such, the target detection problem can be analyzed using the information theory of the relay channel, where a number of information metrics can be defined. It is believed that such analysis could help us to understand the intrinsic nature of the DFRC systems, and point us to the essential system design criteria.

Appendix A
Proof of Proposition 1

Let us denote $\mathbf{F}_0 = [\mathbf{F}_{BS}, \mathbf{F}_{aux}]$, and expand the objective function as

$$\begin{aligned}
&\left\|\mathbf{F}_{RF}\mathbf{F}_{BB} - \mathbf{F}_0\right\|_F^2 \\
&= \mathrm{tr}\left(\left(\mathbf{F}_{RF}\mathbf{F}_{BB} - \mathbf{F}_0\right)\left(\mathbf{F}_{RF}\mathbf{F}_{BB} - \mathbf{F}_0\right)^H\right) \\
&= \mathrm{tr}\left(\mathbf{F}_{RF}\mathbf{F}_{BB}\mathbf{F}_{BB}^H\mathbf{F}_{RF}^H\right) \\
&\quad -2\,\mathrm{Re}\left(\mathrm{tr}\left(\mathbf{F}_0\mathbf{F}_{BB}^H\mathbf{F}_{RF}^H\right)\right) + \mathrm{tr}\left(\mathbf{F}_0\mathbf{F}_0^H\right) \\
&= \frac{P_T}{KN_{BS}}\,\mathrm{tr}\left(\mathbf{F}_{RF}\mathbf{F}_{RF}^H\right) \\
&\quad -2\,\mathrm{Re}\left(\mathrm{tr}\left(\mathbf{F}_0\mathbf{F}_{BB}^H\mathbf{F}_{RF}^H\right)\right) + \mathrm{tr}\left(\mathbf{F}_0\mathbf{F}_0^H\right).
\end{aligned} \tag{77}$$

Based on above, it can be observed that the problem (53) is equivalent to maximizing $\mathrm{Re}\left(\mathrm{tr}\left(\mathbf{F}_0\mathbf{F}_{BB}^H\mathbf{F}_{RF}^H\right)\right)$ under the constraint that $\mathbf{F}_{BB}\mathbf{F}_{BB}^H = \frac{P_T}{KN_{BS}}\mathbf{I}_K$. Let $\tilde{\mathbf{U}}\tilde{\mathbf{\Sigma}}\tilde{\mathbf{V}}^H = \mathbf{F}_{RF}^H\mathbf{F}_0$ be the SVD of $\mathbf{F}_{RF}^H\mathbf{F}_0$, and denote $\mathbf{T} = \tilde{\mathbf{V}}^H\mathbf{F}_{BB}^H\tilde{\mathbf{U}}$. Given the fact that $\tilde{\mathbf{\Sigma}}$ is a diagonal matrix, we have

$$\begin{aligned}
&\mathrm{Re}\left(\mathrm{tr}\left(\mathbf{F}_0\mathbf{F}_{BB}^H\mathbf{F}_{RF}^H\right)\right) = \mathrm{Re}\left(\mathrm{tr}\left(\mathbf{F}_{BB}^H\mathbf{F}_{RF}^H\mathbf{F}_0\right)\right) \\
&= \mathrm{Re}\left(\mathrm{tr}\left(\mathbf{F}_{BB}^H\tilde{\mathbf{U}}\tilde{\mathbf{\Sigma}}\tilde{\mathbf{V}}^H\right)\right) = \mathrm{Re}\left(\mathrm{tr}\left(\tilde{\mathbf{V}}^H\mathbf{F}_{BB}^H\tilde{\mathbf{U}}\tilde{\mathbf{\Sigma}}\right)\right) \\
&= \mathrm{Re}\left(\mathrm{tr}\left(\mathbf{T}\tilde{\mathbf{\Sigma}}\right)\right) = \mathrm{Re}\left(\sum_{k=1}^{K}\mathbf{T}\left(k,k\right)\tilde{\mathbf{\Sigma}}\left(k,k\right)\right).
\end{aligned} \tag{78}$$

Since

$$\mathbf{T}^H\mathbf{T} = \mathbf{F}_{BB}\mathbf{F}_{BB}^H = \frac{P_T}{KN_{BS}}\mathbf{I}_K, \tag{79}$$

we have $\mathbf{T}\left(k,k\right) \le \sqrt{\frac{P_T}{KN_{BS}}}$. It follows that a global maximizer of (78) is given as

$$\mathbf{T} = \tilde{\mathbf{V}}^H\mathbf{F}_{BB}^H\tilde{\mathbf{U}} = \sqrt{\frac{P_T}{KN_{BS}}}\mathbf{I}_K, \tag{80}$$

which indicates that the optimal $\mathbf{F}_{BB}$ is

$$\mathbf{F}_{BB} = \sqrt{\frac{P_T}{KN_{BS}}}\tilde{\mathbf{U}}\tilde{\mathbf{V}}^H. \tag{81}$$

This completes the proof.

Appendix B
Proof of Proposition 2

Let us denote the SVD of $\mathbf{F}_{RF}^H\mathbf{F}_{BS}$ as

$$\mathbf{F}_{RF}^H\mathbf{F}_{BS} = \left[\tilde{\mathbf{U}}_s, \tilde{\mathbf{U}}_n\right]\begin{bmatrix}\tilde{\mathbf{\Sigma}}_s \\ \mathbf{0}\end{bmatrix}\tilde{\mathbf{V}}_s, \tag{82}$$

where $\tilde{\mathbf{U}}_s \in \mathbb{C}^{K\times L}$ and $\tilde{\mathbf{V}}_s \in \mathbb{C}^{L\times L}$ contain the left and right singular vectors associated with non-zero singular values, and $\tilde{\mathbf{U}}_n \in \mathbb{C}^{K\times(K-L)}$ contains the left singular vectors corresponding to zero singular values. We then compute the optimal solution of (53) when $\mathbf{F}_{aux} = \mathbf{0}$. Note that

$$\mathbf{F}_{RF}^H\left[\mathbf{F}_{BS}, \mathbf{F}_{aux}\right] = \left[\tilde{\mathbf{U}}_s, \tilde{\mathbf{U}}_n\right]\begin{bmatrix}\tilde{\mathbf{\Sigma}}_s & \\ & \mathbf{0}\end{bmatrix}\begin{bmatrix}\tilde{\mathbf{V}}_s & \\ & \tilde{\mathbf{V}}_n\end{bmatrix}, \tag{83}$$

which is the SVD of $\mathbf{F}_{RF}^H\left[\mathbf{F}_{BS}, \mathbf{F}_{aux}\right]$ for $\mathbf{F}_{aux} = \mathbf{0}$, where $\tilde{\mathbf{V}}_n$ is an arbitrary $(K-L)\times(K-L)$ unitary matrix. According to Proposition 1, the optimal solution to problem (53) can therefore be obtained in the form

$$\begin{aligned}
\mathbf{F}_{BB} &= \sqrt{\frac{P_T}{KN_{BS}}}\left[\tilde{\mathbf{U}}_s, \tilde{\mathbf{U}}_n\right]\begin{bmatrix}\tilde{\mathbf{V}}_s & \\ & \tilde{\mathbf{V}}_n\end{bmatrix} \\
&= \sqrt{\frac{P_T}{KN_{BS}}}\left[\tilde{\mathbf{U}}_s\tilde{\mathbf{V}}_s, \tilde{\mathbf{U}}_n\tilde{\mathbf{V}}_n\right].
\end{aligned} \tag{84}$$

It follows that

$$\mathbf{F}_{BB,1} = \sqrt{\frac{P_T}{KN_{BS}}}\tilde{\mathbf{U}}_s\tilde{\mathbf{V}}_s, \mathbf{F}_{BB,2} = \sqrt{\frac{P_T}{KN_{BS}}}\tilde{\mathbf{U}}_n\tilde{\mathbf{V}}_n. \tag{85}$$

It can be readily verified that $\mathbf{F}_{BB}$ is indeed a unitary matrix that satisfies the constraint in (53). Furthermore, we have

$$\mathbf{F}_{BB,2}^H\mathbf{F}_{RF}^H\mathbf{F}_{BS} = \sqrt{\frac{P_T}{KN_{BS}}}\tilde{\mathbf{V}}_n^H\tilde{\mathbf{U}}_n^H\mathbf{F}_{RF}^H\mathbf{F}_{BS} = \mathbf{0}, \tag{86}$$

which suggests that

$$\mathbf{F}_{BS}^{H}\mathbf{F}_{RF}\mathbf{F}_{BB,2}=\left(\tilde{\mathbf{H}}\tilde{\mathbf{H}}^{H}\right)^{-1}\tilde{\mathbf{H}}\mathbf{F}_{RF}\mathbf{F}_{BB,2}=\mathbf{0}. \quad (87)$$

By multiplying the above equation with $\mathbf{B}\left(\Phi\right)\tilde{\mathbf{H}}\tilde{\mathbf{H}}^{H}$, we have

$$\mathbf{B}\left(\Phi\right)\tilde{\mathbf{H}}\mathbf{F}_{RF}\mathbf{F}_{BB,2}=\mathbf{H}\mathbf{F}_{RF}\mathbf{F}_{BB,2}=\mathbf{0}. \quad (88)$$

This completes the proof.

REFERENCES

[1] BBC. (2015) Price hike for UK mobile spectrum. [Online]. Available: http://www.bbc.co.uk/news/technology-34346822

[2] A. Morris. (2015) German spectrum auction raises more than 5B. [Online]. Available: https://www.fiercewireless.com/europe/german-spectrum-auction-raises-more-than-eu5b

[3] S. Riaz. (2019) US completes first 5G auction. [Online]. Available: https://www.mobileworldlive.com/featured-content/top-three/us-completes-first-5g-auction/

[4] P. Brown. (2016) 75.4 billion devices connected to the internet of things by 2025. [Online]. Available: https://electronics360.globalspec.com/article/6551/75-4-billion-devices-connected-to-the-internet-of-things-by-2025

[5] H. Griffiths, L. Cohen, S. Watts, E. Mokole, C. Baker, M. Wicks, and S. Blunt, "Radar spectrum engineering and management: Technical and regulatory issues," *Proc. IEEE*, vol. 103, no. 1, pp. 85–102, 2015.

[6] FCC. (2010) Connecting America: The national broadband plan. [Online]. Available: https://www.fcc.gov/general/national-broadband-plan

[7] NSF. (2016) Spectrum efficiency, energy efficiency, and security (specEES): Enabling spectrum for all. [Online]. Available: https://www.nsf.gov/pubs/2016/nsf16616/nsf16616.htm

[8] DARPA. (2016) Shared spectrum access for radar and communications (SSPARC). [Online]. Available: https://www.darpa.mil/program/shared-spectrum-access-for-radar-and-communications

[9] Ofcom. (2015) Public sector spectrum release (PSSR): Award of the 2.3 GHz and 3.4 GHz bands. [Online]. Available: https://www.ofcom.org.uk/consultations-and-statements/category-1/2.3-3.4-ghz-auction-design

[10] CAA. Public sector spectrum release programme: Radar planning and spectrum sharing in the 2.7-2.9GHz bands. [Online]. Available: https://www.caa.co.uk/Commercial-industry/Airspace/Communication-navigation-and-surveillance/Spectrum/Public-sector-spectrum-release-programme/

[11] B. Paul, A. R. Chiriyath, and D. W. Bliss, "Survey of RF communications and sensing convergence research," *IEEE Access*, vol. 5, pp. 252–270, Dec 2017.

[12] H. Wymeersch, G. Seco-Granados, G. Destino, D. Dardari, and F. Tufvesson, "5G mmwave positioning for vehicular networks," *IEEE Wireless Commun.*, vol. 24, no. 6, pp. 80–86, Dec 2017.

[13] C. Yang and H. Shao, "WiFi-based indoor positioning," *IEEE Commun. Mag.*, vol. 53, no. 3, pp. 150–157, Mar 2015.

[14] S. D. Blunt, P. Yatham, and J. Stiles, "Intrapulse radar-embedded communications," *IEEE Trans. Aerosp. Electron. Syst.*, vol. 46, no. 3, pp. 1185–1200, Jul 2010.

[15] H. Wang, J. T. Johnson, and C. J. Baker, "Spectrum sharing between communications and ATC radar systems," *IET Radar Sonar Navig.*, vol. 11, no. 6, pp. 994–1001, Jul 2017.

[16] J. H. Reed, A. W. Clegg, A. V. Padaki, T. Yang, R. Nealy, C. Dietrich, C. R. Anderson, and D. M. Mearns, "On the co-existence of TD-LTE and radar over 3.5 GHz band: An experimental study," *IEEE Wireless Commun. Lett.*, vol. 5, no. 4, pp. 368–371, Aug 2016.

[17] F. Hessar and S. Roy, "Spectrum sharing between a surveillance radar and secondary Wi-Fi networks," *IEEE Trans. Aerosp. Electron. Syst.*, vol. 52, no. 3, pp. 1434–1448, June 2016.

[18] W. Contributors. (2019) List of WLAN channels - Wikipedia, the free encyclopedia. [Online]. Available: https://en.wikipedia.org/wiki/{L}ist_of_{WLAN}_channels

[19] J. Choi, V. Va, N. Gonzalez-Prelcic, R. Daniels, C. R. Bhat, and R. W. Heath, "Millimeter-wave vehicular communication to support massive automotive sensing," *IEEE Commun. Mag.*, vol. 54, no. 12, pp. 160–167, Dec 2016.

[20] W. Roh, J. Seol, J. Park, B. Lee, J. Lee, Y. Kim, J. Cho, K. Cheun, and F. Aryanfar, "Millimeter-wave beamforming as an enabling technology for 5G cellular communications: Theoretical feasibility and prototype results," *IEEE Commun. Mag.*, vol. 52, no. 2, pp. 106–113, Feb 2014.

[21] J. B. Kenney, "Dedicated short-range communications (DSRC) standards in the united states," *Proc. IEEE*, vol. 99, no. 7, pp. 1162–1182, Jul 2011.

[22] T. S. Rappaport, S. Sun, R. Mayzus, H. Zhao, Y. Azar, K. Wang, G. N. Wong, J. K. Schulz, M. Samimi, and F. Gutierrez, "Millimeter wave mobile communications for 5G cellular: It will work!" *IEEE Access*, vol. 1, pp. 335–349, May 2013.

[23] R. W. Heath, N. Gonzlez-Prelcic, S. Rangan, W. Roh, and A. M. Sayeed, "An overview of signal processing techniques for millimeter wave MIMO systems," *IEEE J. Sel. Topics Signal Process.*, vol. 10, no. 3, pp. 436–453, Apr 2016.

[24] C. Xu, B. Firner, Y. Zhang, and R. E. Howard, "The case for efficient and robust RF-based device-free localization," *IEEE Trans. Mobile Comput.*, vol. 15, no. 9, pp. 2362–2375, Sep 2016.

[25] Y. Yoon and M. G. Amin, "Spatial filtering for wall-clutter mitigation in through-the-wall radar imaging," *IEEE Trans. Geosci. Remote Sens.*, vol. 47, no. 9, pp. 3192–3208, Sep 2009.

[26] Lin-Ping Song, Chun Yu, and Qing Huo Liu, "Through-wall imaging (TWI) by radar: 2-D tomographic results and analyses," *IEEE Trans. Geosci. Remote Sens.*, vol. 43, no. 12, pp. 2793–2798, Dec 2005.

[27] C. Feng, W. S. A. Au, S. Valaee, and Z. Tan, "Received-signal-strength-based indoor positioning using compressive sensing," *IEEE Trans. Mobile Comput.*, vol. 11, no. 12, pp. 1983–1993, Dec 2012.

[28] K. Wu, J. Xiao, Y. Yi, D. Chen, X. Luo, and L. M. Ni, "CSI-based indoor localization," *IEEE Trans. Parallel Distrib. Syst.*, vol. 24, no. 7, pp. 1300–1309, Jul 2013.

[29] C. Xu, B. Firner, Y. Zhang, R. Howard, J. Li, and X. Lin, "Improving RF-based device-free passive localization in cluttered indoor environments through probabilistic classification methods," in *2012 ACM/IEEE 11th International Conference on Information Processing in Sensor Networks (IPSN)*, Apr 2012, pp. 209–220.

[30] B. Tan, Q. Chen, K. Chetty, K. Woodbridge, W. Li, and R. Piechocki, "Exploiting WiFi channel state information for residential healthcare informatics," *IEEE Commun. Mag.*, vol. 56, no. 5, pp. 130–137, May 2018.

[31] F. Fioranelli, M. Ritchie, and H. Griffiths, "Bistatic human micro-Doppler signatures for classification of indoor activities," in *2017 IEEE Radar Conference (RadarConf)*, May 2017, pp. 0610–0615.

[32] M. G. Amin, Y. D. Zhang, F. Ahmad, and K. C. D. Ho, "Radar signal processing for elderly fall detection: The future for in-home monitoring," *IEEE Signal Process. Mag.*, vol. 33, no. 2, pp. 71–80, Mar 2016.

[33] Q. Wu, Y. D. Zhang, W. Tao, and M. G. Amin, "Radar-based fall detection based on Doppler timefrequency signatures for assisted living," *IET Radar Sonar Navig.*, vol. 9, no. 2, pp. 164–172, 2015.

[34] C. Dubois. (2019) Google ATAP moves forward with radar touch tech with FCC waiver. [Online]. Available: https://www.allaboutcircuits.com/news/Google-ATAP-Project-Soli-radar-touch-sensor-technology-FCC-waiver/

[35] S. Zhang, Y. Zeng, and R. Zhang, "Cellular-enabled uav communication: A connectivity-constrained trajectory optimization perspective," *IEEE Trans. Commun.*, vol. 67, no. 3, pp. 2580–2604, Mar 2019.

[36] A. Ryan, M. Zennaro, A. Howell, R. Sengupta, and J. K. Hedrick, "An overview of emerging results in cooperative UAV control," in *2004 43rd IEEE Conference on Decision and Control (CDC)*, vol. 1, Dec 2004, pp. 602–607.

[37] Y. Zeng, R. Zhang, and T. J. Lim, "Wireless communications with unmanned aerial vehicles: Opportunities and challenges," *IEEE Commun. Mag.*, vol. 54, no. 5, pp. 36–42, May 2016.

[38] N. Decarli, F. Guidi, and D. Dardari, "A novel joint RFID and radar sensor network for passive localization: Design and performance bounds," *IEEE J. Sel. Topics Signal Process.*, vol. 8, no. 1, pp. 80–95, Feb 2014.

[39] G. Fortino, M. Pathan, and G. D. Fatta, "BodyCloud: Integration of cloud computing and body sensor networks," in *4th IEEE International Conference on Cloud Computing Technology and Science Proceedings*, 2012, pp. 851–856.

[40] D. W. Bliss, "Cooperative radar and communications signaling: The estimation and information theory odd couple," in *2014 IEEE Radar Conference*, May 2014, pp. 0050–0055.

[41] P. K. Hughes and J. Y. Choe, "Overview of advanced multifunction RF system (AMRFS)," in *Proceedings 2000 IEEE International Con-*

ference on Phased Array Systems and Technology (Cat. No.00TH8510), May 2000, pp. 21–24.

[42] G. C. Tavik, C. L. Hilterbrick, J. B. Evins, J. J. Alter, J. G. Crnkovich, J. W. de Graaf, W. Habicht, G. P. Hrin, S. A. Lessin, D. C. Wu, and S. M. Hagewood, "The advanced multifunction RF concept," *IEEE Trans. Microw. Theory Technol.*, vol. 53, no. 3, pp. 1009–1020, Mar 2005.

[43] J. A. Molnar, I. Corretjer, and G. Tavik, "Integrated topside - integration of narrowband and wideband array antennas for shipboard communications," in *2011 - MILCOM 2011 Military Communications Conference*, Nov 2011, pp. 1802–1807.

[44] R. W. Beard, T. W. McLain, D. B. Nelson, D. Kingston, and D. Johanson, "Decentralized cooperative aerial surveillance using fixed-wing miniature UAVs," *Proc. IEEE*, vol. 94, no. 7, pp. 1306–1324, Jul 2006.

[45] R. Schneiderman, "Unmanned drones are flying high in the military/aerospace sector [special reports]," *IEEE Signal Process. Mag.*, vol. 29, no. 1, pp. 8–11, Jan 2012.

[46] Z. R. Bogdanowicz, "Flying swarm of drones over circulant digraph," *IEEE Trans. Aerosp. Electron. Syst.*, vol. 53, no. 6, pp. 2662–2670, Dec 2017.

[47] S. Winkler, S. Zeadally, and K. Evans, "Privacy and civilian drone use: The need for further regulation," *IEEE Security Privacy*, vol. 16, no. 5, pp. 72–80, Sep 2018.

[48] D. B. Ramos, D. S. Loubach, and A. M. da Cunha, "Developing a distributed real-time monitoring system to track UAVs," *IEEE Trans. Aerosp. Electron. Syst.*, vol. 25, no. 9, pp. 18–25, Sep 2010.

[49] S. Zhang, H. Zhang, B. Di, and L. Song, "Cellular UAV-to-X communications: Design and optimization for multi-UAV networks," *IEEE Trans. Wireless Commun.*, vol. 18, no. 2, pp. 1346–1359, Feb 2019.

[50] A. Polydoros and K. Woo, "LPI detection of frequency-hopping signals using autocorrelation techniques," *IEEE J. Sel. Areas Commun.*, vol. 3, no. 5, pp. 714–726, Sep 1985.

[51] A. Polydoros and C. Weber, "Detection performance considerations for direct-sequence and time-hopping LPI waveforms," *IEEE J. Sel. Areas Commun.*, vol. 3, no. 5, pp. 727–744, Sep 1985.

[52] S. D. Blunt, J. G. Metcalf, C. R. Biggs, and E. Perrins, "Performance characteristics and metrics for intra-pulse radar-embedded communication," *IEEE J. Sel. Areas Commun*, vol. 29, no. 10, pp. 2057–2066, Dec 2011.

[53] D. Ciuonzo, A. De Maio, G. Foglia, and M. Piezzo, "Intrapulse radar-embedded communications via multiobjective optimization," *IEEE Trans. Aerosp. Electron. Syst.*, vol. 51, no. 4, pp. 2960–2974, Oct 2015.

[54] S. Brisken, M. Moscadelli, V. Seidel, and C. Schwark, "Passive radar imaging using DVB-S2," in *2017 IEEE Radar Conference (RadarConf)*, May 2017, pp. 0552–0556.

[55] H. Griffiths and C. J. Baker, *An Introduction to Passive Radar*. Artech House, 2017.

[56] J. Liu, H. Li, and B. Himed, "Two target detection algorithms for passive multistatic radar," *IEEE Transactions on Signal Processing*, vol. 62, no. 22, pp. 5930–5939, Nov 2014.

[57] B. K. Chalise, M. G. Amin, and B. Himed, "Performance tradeoff in a unified passive radar and communications system," *IEEE Signal Process. Lett.*, vol. 24, no. 9, pp. 1275–1279, Sep 2017.

[58] L. S. Wang, J. P. Mcgeehan, C. Williams, and A. Doufexi, "Application of cooperative sensing in radar-communications coexistence," *IET Commun.*, vol. 2, no. 6, pp. 856–868, Jul 2008.

[59] R. Saruthirathanaworakun, J. M. Peha, and L. M. Correia, "Opportunistic sharing between rotating radar and cellular," *IEEE J. Sel. Areas Commun.*, vol. 30, no. 10, pp. 1900–1910, Nov 2012.

[60] J. Li and P. Stoica, "MIMO radar with colocated antennas," *IEEE Signal Process. Mag.*, vol. 24, no. 5, pp. 106–114, Sep 2007.

[61] J. Li and P. Stoica, *MIMO radar signal processing*. John Wiley & Sons, 2008.

[62] M. Biguesh and A. B. Gershman, "Training-based MIMO channel estimation: A study of estimator tradeoffs and optimal training signals," *IEEE Trans. Signal Process.*, vol. 54, no. 3, pp. 884–893, Mar 2006.

[63] J. A. Mahal, A. Khawar, A. Abdelhadi, and T. C. Clancy, "Spectral coexistence of MIMO radar and MIMO cellular system," *IEEE Trans. Aerosp. Electron. Syst.*, vol. 53, no. 2, pp. 655–668, Apr 2017.

[64] B. Li and A. P. Petropulu, "Joint transmit designs for coexistence of MIMO wireless communications and sparse sensing radars in clutter," *IEEE Trans. Aerosp. Electron. Syst.*, vol. 53, no. 6, pp. 2846–2864, Dec 2017.

[65] F. Liu, A. Garcia-Rodriguez, C. Masouros, and G. Geraci, "Interfering channel estimation in radar-cellular coexistence: How much information do we need?" *IEEE Trans. Wireless Commun.*, vol. 18, no. 9, pp. 4238–4253, Sep 2019.

[66] A. Khawar, A. Abdelhadi, and C. Clancy, "Target detection performance of spectrum sharing MIMO radars," *IEEE Sensors J.*, vol. 15, no. 9, pp. 4928–4940, Sep 2015.

[67] A. Babaei, W. H. Tranter, and T. Bose, "A nullspace-based precoder with subspace expansion for radar/communications coexistence," in *2013 IEEE Global Communications Conference (GLOBECOM)*, Dec 2013, pp. 3487–3492.

[68] B. Li, A. P. Petropulu, and W. Trappe, "Optimum co-design for spectrum sharing between matrix completion based MIMO radars and a MIMO communication system," *IEEE Trans. Signal Process.*, vol. 64, no. 17, pp. 4562–4575, Sep 2016.

[69] L. Zheng, M. Lops, X. Wang, and E. Grossi, "Joint design of overlaid communication systems and pulsed radars," *IEEE Trans. Signal Process.*, vol. 66, no. 1, pp. 139–154, Jan 2018.

[70] F. Liu, C. Masouros, A. Li, and T. Ratnarajah, "Robust MIMO beamforming for cellular and radar coexistence," *IEEE Wireless Commun. Lett.*, vol. 6, no. 3, pp. 374–377, Jun 2017.

[71] Y. Cui, V. Koivunen, and X. Jing, "Interference alignment based spectrum sharing for MIMO radar and communication systems," in *2018 IEEE 19th International Workshop on Signal Processing Advances in Wireless Communications (SPAWC)*, Jun 2018, pp. 1–5.

[72] Z. Cheng, B. Liao, S. Shi, Z. He, and J. Li, "Co-design for overlaid MIMO radar and downlink MISO communication systems via Cramér - Rao bound minimization," *IEEE Trans. Signal Process.*, vol. 67, no. 24, pp. 6227–6240, Dec 2019.

[73] F. Liu, C. Masouros, A. Li, T. Ratnarajah, and J. Zhou, "MIMO radar and cellular coexistence: A power-efficient approach enabled by interference exploitation," *IEEE Trans. Signal Process.*, vol. 66, no. 14, pp. 3681–3695, Jul 2018.

[74] C. Masouros and G. Zheng, "Exploiting known interference as green signal power for downlink beamforming optimization," *IEEE Trans. Signal Process.*, vol. 63, no. 14, pp. 3628–3640, Jul 2015.

[75] L. Zheng, M. Lops, and X. Wang, "Adaptive interference removal for uncoordinated radar/communication coexistence," *IEEE J. Sel. Topics Signal Process.*, vol. 12, no. 1, pp. 45–60, Feb 2018.

[76] N. Nartasilpa, A. Salim, D. Tuninetti, and N. Devroye, "Communications system performance and design in the presence of radar interference," *IEEE Trans. Commun.*, vol. 66, no. 9, pp. 4170–4185, Sep 2018.

[77] A. R. Chiriyath, B. Paul, G. M. Jacyna, and D. W. Bliss, "Inner bounds on performance of radar and communications co-existence," *IEEE Trans. Signal Process.*, vol. 64, no. 2, pp. 464–474, Jan 2016.

[78] J. R. Guerci, R. M. Guerci, A. Lackpour, and D. Moskowitz, "Joint design and operation of shared spectrum access for radar and communications," in *2015 IEEE Radar Conference (RadarCon)*, May 2015, pp. 0761–0766.

[79] S. M. Kay, *Fundamentals of Statistical Signal Processing, Vol. I: Estimation Theory*. Englewood Cliffs, NJ, USA: Prentice Hall, 1998.

[80] A. R. Chiriyath, B. Paul, and D. W. Bliss, "Radar-communications convergence: Coexistence, cooperation, and co-design," *IEEE Trans. Cogn. Commun. Netw.*, vol. 3, no. 1, pp. 1–12, 2017.

[81] Y. Rong, A. R. Chiriyath, and D. W. Bliss, "MIMO radar and communications spectrum sharing: A multiple-access perspective," in *2018 IEEE 10th Sensor Array and Multichannel Signal Processing Workshop (SAM)*, Jul 2018, pp. 272–276.

[82] N. Levanon and E. Mozeson, *Radar signals*. John Wiley & Sons, 2004.

[83] B. R. Mahafza, *Radar systems analysis and design using MATLAB*. Chapman and Hall/CRC, 2005.

[84] M. A. Richards, *Fundamentals of radar signal processing*. Tata McGraw-Hill Education, 2005.

[85] R. M. Mealey, "A method for calculating error probabilities in a radar communication system," *IEEE Trans. Space Electron. Telemetry*, vol. 9, no. 2, pp. 37–42, Jun 1963.

[86] M. Roberton and E. R. Brown, "Integrated radar and communications based on chirped spread-spectrum techniques," in *Microwave Symposium Digest, 2003 IEEE MTT-S International*, vol. 1, 2003, pp. 611–614.

[87] G. N. Saddik, R. S. Singh, and E. R. Brown, "Ultra-wideband multifunctional communications/radar system," *IEEE Trans. Microw. Theory Technol.*, vol. 55, no. 7, pp. 1431–1437, Jul 2007.

[88] M. Jamil, H.-J. Zepernick, and M. I. Pettersson, "On integrated radar and communication systems using Oppermann sequences," in *Proc. IEEE Military Commun.*, 2008, pp. 1–6.

[89] L. Han and K. Wu, "Joint wireless communication and radar sensing systems-state of the art and future prospects," *IET Microw. Antennas Propag.*, vol. 7, no. 11, pp. 876–885, 2013.

[90] D. Garmatyuk, J. Schuerger, and K. Kauffman, "Multifunctional software-defined radar sensor and data communication system," *IEEE Sensors J.*, vol. 11, no. 1, pp. 99–106, Jan 2011.

[91] C. Sturm and W. Wiesbeck, "Waveform design and signal processing aspects for fusion of wireless communications and radar sensing," *Proc. IEEE*, vol. 99, no. 7, pp. 1236–1259, Jul 2011.

[92] D. Gaglione, C. Clemente, C. V. Ilioudis, A. R. Persico, I. K. Proudler, and J. J. Soraghan, "Fractional fourier based waveform for a joint radar-communication system," in *2016 IEEE Radar Conference (RadarConf)*, May 2016, pp. 1–6.

[93] L. B. Almeida, "The fractional Fourier transform and time-frequency representations," *IEEE Trans. Signal Process.*, vol. 42, no. 11, pp. 3084–3091, Nov 1994.

[94] A. J. Paulraj and T. Kailath, "Increasing capacity in wireless broadcast systems using distributed transmission/directional reception (DTDR)," Sep 1994, US Patent 5,345,599.

[95] G. Foschini and M. Gans, "On limits of wireless communications in a fading environment when using multiple antennas," *Wireless Personal Commun.*, vol. 6, no. 3, pp. 311–335, Mar 1998.

[96] E. Telatar, "Capacity of multi-antenna gaussian channels," *European Trans. Telecommun.*, vol. 10, no. 6, pp. 585–595, 1999.

[97] R. L. Walker, "Alvarez: Adventures of a physicist," *Science*, vol. 240, no. 4855, pp. 1065–1067, 1988.

[98] H. Griffiths, "The MAMMUT phased array radar: Compulsive hoarding," in *Proc. International Radar Conference (RADAR)*, Sept. 2019, pp. 23–27.

[99] E. Fishler, A. Haimovich, R. Blum, D. Chizhik, L. Cimini, and R. Valenzuela, "MIMO radar: an idea whose time has come," in *Proceedings of the 2004 IEEE Radar Conference (IEEE Cat. No.04CH37509)*, Apr 2004, pp. 71–78.

[100] F. Daum and J. Huang, "MIMO radar: Snake oil or good idea?" *IEEE Trans. Aerosp. Electron. Syst.*, vol. 24, no. 5, pp. 8–12, May 2009.

[101] R. Schmidt, "Multiple emitter location and signal parameter estimation," in *Proc. RADC Spectrum Estimation Workshop*, Oct. 1979, Rome Air Development Center, Rome, NY, USA; reprinted in *IEEE Trans. Antennas Propag.*, vol. 34, Mar. 1986, pp. 276-280.

[102] R. Roy and T. Kailath, "ESPRIT-estimation of signal parameters via rotational invariance techniques," *IEEE Trans. Acoust., Speech, Signal Process.*, vol. 37, no. 7, pp. 984–995, Jul 1989.

[103] J. Capon, "High-resolution frequency-wavenumber spectrum analysis," *Proc. IEEE*, vol. 57, no. 8, pp. 1408–1418, Aug 1969.

[104] J. Li and P. Stoica, "An adaptive filtering approach to spectral estimation and SAR imaging," *IEEE Trans. Signal Process.*, vol. 44, no. 6, pp. 1469–1484, Jun 1996.

[105] L. Xu, J. Li, and P. Stoica, "Target detection and parameter estimation for MIMO radar systems," *IEEE Trans. Aerosp. Electron. Syst.*, vol. 44, no. 3, pp. 927–939, Jul 2008.

[106] A. Hassanien, M. G. Amin, Y. D. Zhang, and F. Ahmad, "Dual-function radar-communications: Information embedding using sidelobe control and waveform diversity," *IEEE Trans. Signal Process.*, vol. 64, no. 8, pp. 2168–2181, Apr 2016.

[107] A. Hassanien, M. G. Amin, Y. D. Zhang, F. Ahmad, and B. Himed, "Non-coherent psk-based dual-function radar-communication systems," in *2016 IEEE Radar Conference (RadarConf)*, May 2016, pp. 1–6.

[108] E. BouDaher, A. Hassanien, E. Aboutanios, and M. G. Amin, "Towards a dual-function MIMO radar-communication system," in *2016 IEEE Radar Conference (RadarConf)*, May 2016, pp. 1–6.

[109] F. Liu, C. Masouros, A. Li, H. Sun, and L. Hanzo, "MU-MIMO communications with MIMO radar: From co-existence to joint transmission," *IEEE Trans. Wireless Commun.*, vol. 17, no. 4, pp. 2755–2770, Apr 2018.

[110] F. Liu, L. Zhou, C. Masouros, A. Li, W. Luo, and A. Petropulu, "Toward dual-functional radar-communication systems: Optimal waveform design," *IEEE Trans. Signal Process.*, vol. 66, no. 16, pp. 4264–4279, Aug 2018.

[111] F. Liu, C. Masouros, and H. Griffiths, "Dual-functional radar-communication waveform design under constant-modulus and orthogonality constraints," in *2019 Sensor Signal Processing for Defence (SSPD)*, May 2019.

[112] P. Kumari, J. Choi, N. Gonzlez-Prelcic, and R. W. Heath, "IEEE 802.11ad-based radar: An approach to joint vehicular communication-radar system," *IEEE Trans. Veh. Technol.*, vol. 67, no. 4, pp. 3012–3027, Apr 2018.

[113] E. Grossi, M. Lops, L. Venturino, and A. Zappone, "Opportunistic radar in IEEE 802.11ad networks," *IEEE Trans. Signal Process.*, vol. 66, no. 9, pp. 2441–2454, May 2018.

[114] S. Fortunati, L. Sanguinetti, F. Gini, and M. S. Greco. (2019) Massive MIMO radar for target detection. [Online]. Available: https://arxiv.org/abs/1906.06191

[115] X. Zhang, A. F. Molisch, and Sun-Yuan Kung, "Variable-phase-shift-based RF-baseband codesign for MIMO antenna selection," *IEEE Trans. Signal Process.*, vol. 53, no. 11, pp. 4091–4103, Nov 2005.

[116] O. E. Ayach, S. Rajagopal, S. Abu-Surra, Z. Pi, and R. W. Heath, "Spatially sparse precoding in millimeter wave MIMO systems," *IEEE Trans. Wireless Commun.*, vol. 13, no. 3, pp. 1499–1513, Mar 2014.

[117] S. Han, C. I, Z. Xu, and C. Rowell, "Large-scale antenna systems with hybrid analog and digital beamforming for millimeter wave 5G," *IEEE Commun. Mag.*, vol. 53, no. 1, pp. 186–194, Jan 2015.

[118] A. F. Molisch, V. V. Ratnam, S. Han, Z. Li, S. L. H. Nguyen, L. Li, and K. Haneda, "Hybrid beamforming for massive MIMO: A survey," *IEEE Commun. Mag.*, vol. 55, no. 9, pp. 134–141, Sep 2017.

[119] A. Alkhateeb, J. Mo, N. Gonzalez-Prelcic, and R. W. Heath, "MIMO precoding and combining solutions for millimeter-wave systems," *IEEE Commun. Mag.*, vol. 52, no. 12, pp. 122–131, Dec 2014.

[120] A. Hassanien and S. A. Vorobyov, "Phased-MIMO radar: A tradeoff between phased-array and mimo radars," *IEEE Trans. Signal Process.*, vol. 58, no. 6, pp. 3137–3151, Jun 2010.

[121] D. Wilcox and M. Sellathurai, "On MIMO radar subarrayed transmit beamforming," *IEEE Trans. Signal Process.*, vol. 60, no. 4, pp. 2076–2081, Apr 2012.

[122] T. L. Marzetta, "Noncooperative cellular wireless with unlimited numbers of base station antennas," *IEEE Trans. Wireless Commun.*, vol. 9, no. 11, pp. 3590–3600, Nov 2010.

[123] J. A. Zhang, X. Huang, Y. J. Guo, J. Yuan, and R. W. Heath, "Multibeam for joint communication and radar sensing using steerable analog antenna arrays," *IEEE Trans. Veh. Technol.*, vol. 68, no. 1, pp. 671–685, Jan 2019.

[124] W. Roberts, P. Stoica, J. Li, T. Yardibi, and F. A. Sadjadi, "Iterative adaptive approaches to MIMO radar imaging," *IEEE J. Sel. Topics Signal Process.*, vol. 4, no. 1, pp. 5–20, Feb 2010.

[125] D. Zhang, Y. Wang, X. Li, and W. Xiang, "Hybridly connected structure for hybrid beamforming in mmwave massive MIMO systems," *IEEE Trans. Commun.*, vol. 66, no. 2, pp. 662–674, Feb 2018.

[126] N. Gonzlez-Prelcic, R. Mndez-Rial, and R. W. Heath, "Radar aided beam alignment in mmWave V2I communications supporting antenna diversity," in *Proc. Information Theory and Applications Workshop (ITA)*, Jan 2016, pp. 1–7.

[127] H. Jiang, J. Zhang, and K. M. Wong, "Joint DOD and DOA estimation for bistatic MIMO radar in unknown correlated noise," *IEEE Trans. Veh. Technol.*, vol. 64, no. 11, pp. 5113–5125, Nov 2015.

[128] G. Berardinelli, K. I. Pedersen, F. Frederiksen, and P. Mogensen, "On the guard period design in 5G TDD wide area," in *2016 IEEE 83rd Vehicular Technology Conference (VTC Spring)*, May 2016, pp. 1–5.

[129] D. Tse and P. Viswanath, *Fundamentals of wireless communication*. Cambridge university press, 2005.

[130] O. Aldayel, V. Monga, and M. Rangaswamy, "Successive QCQP refinement for MIMO radar waveform design under practical constraints," *IEEE Trans. Signal Process.*, vol. 64, no. 14, pp. 3760–3774, Jul 2016.

[131] CustomMMIC. (2019) High performance RF/microwave GaAs MMIC switches for SPST, SPDT, SP3T, SP4T, and SP5T switching requirements. [Online]. Available: https://www.custommmic.com/mmic-switches/

[132] R. Schmidt, "Multiple emitter location and signal parameter estimation," *IEEE Trans. Antennas Propag.*, vol. 34, no. 3, pp. 276–280, Mar 1986.

[133] Y. Ge, W. Zhang, F. Gao, and H. Minn, "Angle-domain approach for parameter estimation in high-mobility ofdm with fully/partly calibrated massive ULA," *IEEE Trans. Wireless Commun.*, vol. 18, no. 1, pp. 591–607, Jan 2019.

[134] W. Guo, W. Zhang, P. Mu, F. Gao, and H. Lin, "High-mobility wideband massive MIMO communications: Doppler compensation, analysis and scaling laws," *IEEE Trans. Wireless Commun.*, vol. 18, no. 6, pp. 3177–3191, Jun 2019.

[135] Y. Zeng, L. Yang, and R. Zhang, "Multi-user millimeter wave MIMO with full-dimensional lens antenna array," *IEEE Trans. Wireless Commun.*, vol. 17, no. 4, pp. 2800–2814, Apr 2018.

[136] G. Wang, J. Sun, and G. Ascheid, "Hybrid beamforming with time delay compensation for millimeter wave MIMO frequency selective channels," in *2016 IEEE 83rd Vehicular Technology Conference (VTC Spring)*, May 2016, pp. 1–6.

[137] A. Deligiannis, A. Daniyan, S. Lambotharan, and J. A. Chambers, "Secrecy rate optimizations for MIMO communication radar," *IEEE Trans. Aerosp. Electron. Syst.*, vol. 54, no. 5, pp. 2481–2492, Oct 2018.

[138] B. K. Chalise and M. G. Amin, "Performance tradeoff in a unified system of communications and passive radar: A secrecy capacity approach," *Digital Signal Process.*, vol. 82, pp. 282 – 293, 2018.
[139] A. Dimas, M. A. Clark, K. Psounis, and A. P. Petropulu, "On radar privacy in shared spectrum scenarios," in *2019 IEEE International Conference on Acoustics, Speech and Signal Processing (ICASSP)*, May 2019.
[140] S. H. Dokhanchi, B. S. Mysore, K. V. Mishra, and B. Ottersten, "A mmWave automotive joint radar-communications system," *IEEE Trans. Aerosp. Electron. Syst.*, pp. 1–1, 2019.
[141] S. Shahi, D. Tuninetti, and N. Devroye, "On the capacity of the AWGN channel with additive radar interference," *IEEE Trans. Commun.*, vol. 66, no. 2, pp. 629–643, Feb 2018.

Fan Liu (S'16-M'18) received the Ph.D. and the BEng. degrees from Beijing Institute of Technology (BIT), Beijing, China, in 2018 and 2013, respectively. He has been a visiting Ph.D. student in the Department of Electronics and Electrical Engineering, University College London (UCL) between 2016-2018, where he is currently a Marie Curie Research Fellow. He was the recipient of the Best Ph.D. Thesis Award of Chinese Institute of Electronics in 2019, and the Marie Curie Individual Fellowship in 2018. He has been named as an Exemplary Reviewer for the IEEE Transactions on Wireless Communications, the IEEE Transactions on Communications and the IEEE Communications Letters. He has served as the Co-Chair of the IEEE ICC 2020 Workshop on Communication and Radar Spectrum Sharing. His research interests include vehicular network, massive MIMO and mmWave communications, and radar signal processing.

Christos Masouros (M'06-SM'14) received the Diploma degree in Electrical and Computer Engineering from the University of Patras, Greece, in 2004, and MSc by research and PhD in Electrical and Electronic Engineering from the University of Manchester, UK in 2006 and 2009 respectively. In 2008 he was a research intern at Philips Research Labs, UK. Between 2009-2010 he was a Research Associate in the University of Manchester and between 2010-2012 a Research Fellow in Queen's University Belfast. In 2012 he joined University College London as a Lecturer. He has held a Royal Academy of Engineering Research Fellowship between 2011-2016.

He is currently a Full Professor in the Information and Communication Engineering research group, Department of Electrical and Electronic Engineering, and affiliated with the Institute for Communications and Connected Systems, University College London. His research interests lie in the field of wireless communications and signal processing with particular focus on Green Communications, Large Scale Antenna Systems, Communications and Radar Co-existence, interference mitigation techniques for MIMO and multi-carrier communications. He was the recipient of the Best Paper Awards in the IEEE Globecom 2015 and IEEE WCNC 2019 conferences, and has been recognized as an Exemplary Editor for the IEEE Communications Letters, and as an Exemplary Reviewer for the IEEE Transactions on Communications. He is an Editor for IEEE Transactions on Communications, IEEE Transactions on Wireless Communications and IEEE Open Journal of Signal Processing. He has been an Associate Editor for IEEE Communications Letters, and a Guest Editor for IEEE Journal on Selected Topics in Signal Processing issues "Exploiting Interference towards Energy Efficient and Secure Wireless Communications" and "Hybrid Analog / Digital Signal Processing for Hardware-Efficient Large Scale Antenna Arrays". He is currently an elected member of the EURASIP SAT Committee on Signal Processing for Communications and Networking.

Athina P. Petropulu (F'08) received her undergraduate degree from the National Technical University of Athens, Greece, and the M.Sc. and Ph.D. degrees from Northeastern University, Boston MA, all in Electrical and Computer Engineering. She is Distinguished Professor at the Electrical and Computer Engineering (ECE) Department at Rutgers, having served as chair of the department during 2010-2016. Before joining Rutgers in 2010, she was faculty at Drexel University. She held Visiting Scholar appointments at SUPELEC, Universite' Paris Sud, Princeton University and University of Southern California. Dr. Petropulu's research interests span the area of statistical signal processing, wireless communications, signal processing in networking, physical layer security, and radar signal processing. Her research has been funded by various government industry sponsors including the National Science Foundation (NSF), the Office of Naval research, the US Army, the National Institute of Health, the Whitaker Foundation, Lockheed Martin and Raytheon.

Dr. Petropulu is Fellow of IEEE and AAAS and recipient of the 1995 Presidential Faculty Fellow Award given by NSF and the White House. She is President-Elect for the IEEE Signal Processing Society for 2020-2021. She has served as Editor-in-Chief of the IEEE Transactions on Signal Processing (2009-2011), IEEE Signal Processing Society Vice President-Conferences (2006-2008), and is currently member-at-large of the IEEE Signal Processing Board of Governors. She was the General Chair of the 2005 International Conference on Acoustics Speech and Signal Processing (ICASSP-05), Philadelphia PA, and is General Co-Chair of the 2018 IEEE International Workshop on Signal Processing Advances in Wireless Communications (SPAWC). She is recipient of the 2005 IEEE Signal Processing Magazine Best Paper Award, and the 2012 IEEE Signal Processing Society Meritorious Service Award. She was Distinguished Lecturer for the Signal Processing Society for 2017-2018, and is currently Distinguished Lecturer for the IEEE Aerospace & Electronics Systems Society.

Hugh Griffiths (M'86-SM'90-F'99) received his M.A. degree in physics from Oxford University in 1975. He received a Ph.D. degree in 1986 and a D.Sc. (Eng.) degree in 2000, both from University College London. He holds the THALES/Royal Academy Chair of RF Sensors in the Department of Electronic and Electrical Engineering at University College London, England. From 2006-2008 he was the Principal of the Defence Academy of Management and Technology, Shrivenham. From 2001-2006 he was Head of Department at University College London. His research interests include radar and sonar systems, signal processing (particularly synthetic aperture radar and bistatic and multistatic radar), and antenna measurement techniques. He carried out some of the first experiments in passive bistatic radar.

Dr. Griffiths has published over five hundred papers and technical articles in the fields of radar, antennas, and sonar. He received the IEEE AESS Nathanson Award (1996), the IET A F Harvey Research Prize (2013) and the IEEE Picard Medal (2017). He has also received the Brabazon Premium of the IERE and the Mountbatten and Maxwell Premium Awards of the IEE. He is a Fellow of the IET, and in 1997, he was elected to Fellowship of the Royal Academy of Engineering. He served as President of the IEEE Aerospace and Electronic Systems Society for 2012-2013. He has been a member of the IEEE AES Radar Systems Panel since 1989, serving as chair from 2007-2009, and he chaired the working group which revised the IEEE Radar Definitions Standard P686 and reaffirmed the Radar Letter Band Standard in 2008. He was appointed Officer of the Order of the British Empire (OBE) in the 2019 Queen's New Year's Honours List.

Lajos Hanzo (M'91-SM'92-F'04) received his 5-year Master degree in Electronics in 1976 and his doctoral degree in 1983. In 2004 the University of Southampton bestowed the Doctor of Science (DSc) higher research degree upon him. During his 44-year career in Telecommunications, he has held various research and academic positions in Hungary, Germany. and U.K. Since 1986, he has been with the School of Electronics and Computer Science, University of Southampton, U.K., where he holds the Chair of Telecommunications. He has successfully supervised 119 Ph.D. students, coauthored 18 John Wiley/IEEE Press books on mobile radio communications, totaling in excess of 10,000 pages, published 1477 research papers at IEEE Xplore, acted as TPC and the General Chair of IEEE conferences, presented keynote lectures, and has been awarded a number of distinctions. He is currently directing an academic research team, working on a range of research projects in the field of wireless multimedia communications, sponsored by industry, the Engineering and Physical Sciences Research Council (EPSRC), U.K., the European Research Councils Advanced Fellow Grant, and the Royal Society, UK. He is an enthusiastic supporter of industrial and academic liaison, and he offers a range of industrial courses. He is a Fellow of the Royal Academy of Evgineering (FREng), Fellow of the Institute of Engineering & Technology (FIET), Fellow of the European Signal Processing Association (EURASIP). In 2009, he received an Honorary Doctorate from the Technical University of Budapest, and again in 2015 by from University of Edinburgh. From 2008 to 2012, he was the Editor-in-Chief of the IEEE Press and a Chaired Professor at Tsinghua University, Beijing. His research is funded by the European Research Councils 2.5M-Euro Advanced Fellow Grant. He is a Governor of the IEEE VTS.